
TAB-DRW: A DFT-BASED ROBUST WATERMARK FOR GENERATIVE TABULAR DATA

Yizhou Zhao¹ Xiang Li¹ Peter Song² Qi Long¹ Weijie Su¹

¹University of Pennsylvania ²University of Michigan

November 27, 2025

ABSTRACT

The rise of generative AI has enabled the production of high-fidelity synthetic tabular data across fields such as healthcare, finance, and public policy, raising growing concerns about data provenance and misuse. Watermarking offers a promising solution to address these concerns by ensuring the traceability of synthetic data, but existing methods face many limitations: they are computationally expensive due to reliance on large diffusion models, struggle with mixed discrete-continuous data, or lack robustness to post-modifications. To address them, we propose TAB-DRW, an efficient and robust post-editing watermarking scheme for generative tabular data. TAB-DRW embeds watermark signals in the frequency domain: it normalizes heterogeneous features via the Yeo-Johnson transformation and standardization, applies the discrete Fourier transform (DFT), and adjusts the imaginary parts of adaptively selected entries according to precomputed pseudorandom bits. To further enhance robustness and efficiency, we introduce a novel rank-based pseudorandom bit generation method that enables row-wise retrieval without incurring storage overhead. Experiments on five benchmark tabular datasets show that TAB-DRW achieves strong detectability and robustness against common post-processing attacks, while preserving high data fidelity and fully supporting mixed-type features.

1 Introduction

Tabular data is a predominant format for structured information in many fields such as healthcare, finance, and public policy [6]. It facilitates tasks such as decision-making, risk assessment, and resource allocation. However, access to high-quality tabular data is often restricted by privacy concerns, regulatory constraints on data sharing, and the cost of human annotation. Recent advances in generative AI have revolutionized synthetic data generation [36, 44, 42, 21, 17, 40, 9, 31], which creates high-fidelity tabular datasets that closely match real-world data. Synthetic tabular data now offers a compelling alternative for data sharing and model training in various domains [3].

Despite its benefits, synthetic tabular data also introduces new risks. Misuse can lead to civil disputes, regulatory violations, or societal harm [10]. For instance, generating synthetic datasets from copyrighted materials without authorization may infringe intellectual property rights [30]; in finance, synthetic transaction records can facilitate fraud [2]; in healthcare, biased or inaccurate synthetic patient data can mislead clinical decisions and cause harmful consequences [25]. As synthetic data becomes increasingly realistic and widespread, ensuring accountability and provenance has become critical [20].

To address concerns surrounding the misuse of synthetic tabular data, watermarking has emerged as a promising solution. The core idea is to embed invisible statistical signals into synthetic data before release, allowing reliable detection by a verifier with access to secretly shared information. An effective watermarking scheme should satisfy four key properties: 1) **fidelity**, preserving the quality and utility of the data; 2) **detectability**, allowing reliable identification through a private detection process; 3) **applicability**, enabling efficient watermark embedding even after data generation and for mixed discrete-continuous tabular data; and 4) **robustness**, ensuring resilience against post-processing attacks such

Emails: yzzhao@sas.upenn.edu, 1x10077@upenn.edu, pxsong@umich.edu, qlong@upenn.edu, and suw@wharton.upenn.edu. code is available at <https://github.com/zhyzmath/TAB-DRW-Tabular-Data-Watermarking>.

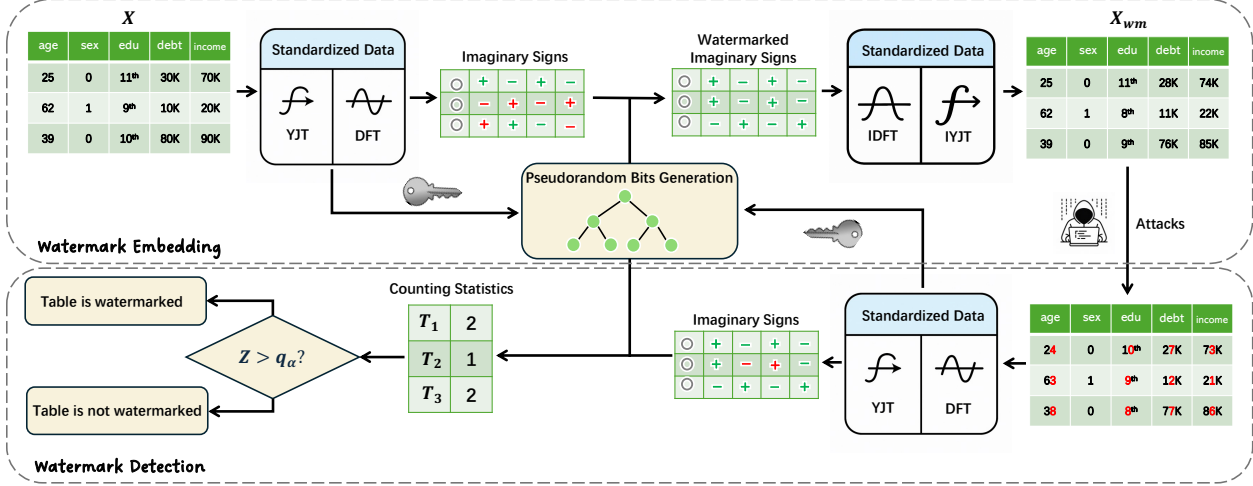


Figure 1: Our proposed watermarking scheme, TAB-DRW, embeds watermarks into tabular data by modifying the imaginary components of the frequency-domain representation to align with pseudorandom bits. Detection evaluates the degree of alignment: strong alignment indicates watermarked data, while weak alignment suggests non-watermarked data.

Table 1: Comparison of our method with existing works. \circ indicates “not satisfied”, \bullet indicates “partially satisfied”, and \blacksquare indicates “satisfied”.

Methods	Category	Data type	Fidelity	Detectability	Applicability	Robustness
TabWak [46]	Sampling-phase	Continuous & Discrete	\blacksquare	\bullet	\circ	\circ
MUSE [8]	Sampling-phase	Continuous & Discrete	\bullet	\bullet	\bullet	\circ
GLW [11]	Post-editing	Only continuous	\bullet	\bullet	\circ	\circ
TabularMark [45]	Post-editing	Continuous & Discrete	\bullet	\bullet	\circ	\circ
TAB-DRW (Ours)	Post-editing	Continuous & Discrete	\bullet	\bullet	\blacksquare	\bullet

as deletions or value modifications [24, 18]. Although significant progress has been made in watermarking text data [15, 18, 43] and images [32, 37, 41], existing watermarking schemes for synthetic tabular data fail to simultaneously achieve these four properties.

Existing works. Current approaches to watermarking synthetic tabular data mainly fall into two categories: sampling-phase watermarking [46, 8] and post-editing watermarking [11, 45]. Sampling-phase methods typically change the sampling process of large diffusion models. Specifically, [46] embeds watermark signals into structured latent noise and detects the structure by measuring correlations with noise reconstructed via the inverse process. While achieving high fidelity and robustness, it relies on reversible sampling strategies, such as DDIM [28], which is prone to reconstruction errors and computationally expensive. [8] generates multiple samples at the same time and outputs the one with the highest pseudorandom score, which incurs higher computational cost though preserving generation quality. In contrast, post-editing methods are lightweight: they often modify generated or existing datasets with pseudorandom operations, but don’t change the sampling process or invoke large neural networks. For example, [11] proposes a “green list” watermark that bins each tabular value into key-selected intervals and detects whether values fall into the designated sets. Although effective in preserving fidelity and detectability, it struggles with mixed-type (continuous and discrete) data and lacks robustness against noise attacks. [45] embeds watermark signals by perturbing key cells with values randomly selected from the so-called “green domain”. However, it requires storing the original dataset for perturbation recovery, leading to substantial space overhead in generative settings. Overall, existing methods offer valuable insights but fall short of providing a lightweight, robust, and broadly applicable solution for synthetic tabular data. See Appendix A for more details on related work.

Our contribution. In this work, we propose a new watermarking method that simultaneously satisfies the four desired properties above. Our contributions are summarized below.

- A new watermarking scheme.** We propose TAB-DRW, a post-editing watermarking method that embeds robust watermark signals in the frequency domain (see Figure 1 for the workflow and Section 2 for the formal introduction). Specifically, it modifies the discrete Fourier transform (DFT) representation of tabular data to align with a precomputed pseudorandom bit sequence. Detection then evaluates the degree of alignment: strong alignment indicates watermarked data, while weak alignment suggests non-watermarked data. TAB-DRW is computationally efficient, requires no model access, and is applicable to both existing and generative tabular data while preserving data fidelity with minimal distortion. Optional rounding and outlier clipping are used to support mixed-type tabular data.
- A new pseudorandom bit generation method.** We introduce a rank-based pseudorandom bit generation scheme to further enhance robustness against post-processing attacks (see Figure 2; detailed in Section 2). This scheme ensures that small modifications to the tabular data do not change the underlying pseudorandom bits. It is also efficient; during detection, pseudorandom bits are retrieved by querying an implicit storage structure based on robust statistics computed from key-selected columns.
- Theoretical analysis and empirical validation.** We provide theoretical insights into the bias and robustness of TAB-DRW. In particular, we show that the embedded watermark signals remain detectable under moderate post-modification. Empirically, we evaluate TAB-DRW using TabSyn [40] as the synthetic data generator. Experiments across five benchmark tabular datasets demonstrate that TAB-DRW achieves superior detectability and robustness, while preserving high data fidelity compared to existing methods.

2 Method

2.1 Watermark Embedding

High-level description. As shown in Figure 1, the embedding process can be divided into three steps. It begins by preprocessing the given tabular data through two transformations: first, a column-wise Yeo-Johnson transformation (YJT) [39] with standardization to reduce heterogeneity and unify the scale; second, a row-wise discrete Fourier transform (DFT) [23] to map the data into the frequency domain. Next, the algorithm modifies the imaginary components of the frequency-domain representation to align with a precomputed pseudorandom bit sequence. Finally, it applies the inverse transformations and un-shuffling to reconstruct the modified data in the original domain, which is then released for public use and future detection. We provide a detailed explanation of these steps below.¹²

Definition 1 (YJT). *For an input $x \in \mathbb{R}$, the YJT $\Psi(\lambda, x)$ is defined as*

$$\Psi(\lambda, x) = \begin{cases} \frac{(x+1)^\lambda - 1}{\lambda}, & \text{if } x \geq 0, \lambda \neq 0, \\ \ln(x+1), & \text{if } x \geq 0, \lambda = 0, \\ -\frac{(-x+1)^{2-\lambda} - 1}{2-\lambda}, & \text{if } x < 0, \lambda \neq 2, \\ -\ln(-x+1), & \text{if } x < 0, \lambda = 2. \end{cases}$$

Here, λ is a transformation parameter that is automatically selected to reduce heterogeneity [27].

Definition 2 (DFT and IDFT). *Given a row of tabular data $\mathbf{x} = (x_0, \dots, x_{p-1}) \in \mathbb{R}^p$, its DFT is defined as $\mathbf{y} = \text{DFT}(\mathbf{x}) := (y_0, \dots, y_{p-1}) \in \mathbb{C}^p$ where $y_t = \frac{1}{\sqrt{p}} \sum_{n=0}^{p-1} x_n e^{-i \frac{2\pi}{p} tn}$ for each $t = 0, \dots, p-1$. The inverse DFT (IDFT) is given by $\mathbf{x} = \text{IDFT}(\mathbf{y}) \in \mathbb{R}^p$ where $x_n = \frac{1}{\sqrt{p}} \sum_{k=0}^{p-1} y_k e^{i \frac{2\pi}{p} kn}$ for each $n = 0, \dots, p-1$. Since $\text{IDFT} \circ \text{DFT} = \text{Id}$, their composition implies an exact recovery of the original input.*

Step 1: Column-wise and row-wise transformations. In general, features in a tabular dataset exhibit heterogeneous scales and types (continuous or discrete). This heterogeneity would prevent a uniform watermarking process among features, as features with larger magnitudes could dominate others. To address this, we first apply a column-wise YJT defined in Def. 1, and then standardize each transformed column. A crucial property of YJT is that it is monotonic and invertible, allowing for exact recovery of the original data through its inverse. After the YJT followed by standardization, each row becomes a real-valued sequence with unified scale. We then apply a row-wise DFT to obtain the frequency-domain representation $\mathbf{y} = \text{DFT}(\mathbf{x}) \in \mathbb{C}^p$, as defined in Def. 2.

Step 2: Modification on the imaginary parts of the DFT. Let $\mathbf{x} := (x_0, x_1, \dots, x_{p-1})$ denote a row of tabular data $\mathbf{X} \in \mathbb{R}^{N \times p}$ after applying the YJT and standardization. Let $\mathbf{y} := \text{DFT}(\mathbf{x}) = (y_0, y_1, \dots, y_{p-1})$ be its frequency-domain representation obtained by the DFT. Since the DFT satisfies conjugate symmetry, i.e., $y_t = \overline{y_{p-t}}$ for any t , it suffices

¹Throughout this paper, we denote the imaginary unit by i , to avoid confusion with the index i .

²We also introduce a privacy-enhanced variant to support multi-key scenarios. See Appendix B & G.4 for details.

Algorithm 1 Watermark embedding of TAB-DRW

- 1: **Input:** Tabular data $\mathbf{X} \in \mathbb{R}^{N \times p}$, parameters $\gamma \in [0, 1]$ and $\delta \in [-1, 1]$.
 - 2: **Initial:** Transform \mathbf{X} using YJT and standardization (still denoted as \mathbf{X} for simplicity).
 - 3: **for** each row \mathbf{x} in \mathbf{X} **do**
 - 4: Compute $\mathbf{y} \leftarrow \text{DFT}(\mathbf{x})$ and generate pseudorandom bits $\{\zeta_t\}_{t=1}^m$ via Algorithm 3.
 - 5: Modify \mathbf{y} according to soft variant (2) to obtain \mathbf{y}^{wm} .
 - 6: Recover $\mathbf{x}^{\text{wm}} \leftarrow \text{IDFT}(\mathbf{y}^{\text{wm}})$.
 - 7: **end for**
 - 8: Collect each \mathbf{x}^{wm} to form a matrix \mathbf{X}^{wm} .
 - 9: Apply inverse standardization and inverse YJT to \mathbf{X}^{wm} , round and clip if needed, and release.
-

to modify only the first half of the entries (i.e. $m = \lfloor \frac{p-1}{2} \rfloor$ entries), as the remaining values can be determined by conjugate symmetry. We call the first m entries effective entries. For each entry y_t , we denote its real and imaginary parts by $\Re(y_t)$ and $\Im(y_t)$ respectively (as $y_t \in \mathbb{C}$). For each effective entry, we generate a 0-1 pseudorandom bit $\zeta_t \sim \text{Bernoulli}(0.5)$ and modify $\Im(y_t)$ to align with the corresponding ζ_t . We consider two modification strategies, described below.

Initial idea: Hard sign flip. The most natural strategy is to force the sign of $\Im(y_t)$ to match ζ_t . Specifically, for each $t = 1, \dots, m$, we define:

$$y_t^{\text{wm}} = \Re(y_t) + (2\zeta_t - 1)\mathbf{i} \cdot |\Im(y_t)|, \quad \text{and} \quad y_{p-t}^{\text{wm}} = \overline{y_t^{\text{wm}}}. \quad (1)$$

Under this rule, if $\Im(y_t)$ already matches the sign of ζ_t , no change is made and $y_t^{\text{wm}} = y_t$. Otherwise, the sign of $\Im(y_t)$ is flipped so that $\Im(y_t^{\text{wm}}) = -\Im(y_t)$.

Refinement: Soft variant. The hard sign flipping may potentially introduce large distortions, degrading data fidelity. As a refinement, we introduce a softer modification controlled by two soft hyperparameters (γ, δ) . Specifically, we modify y_t only if $|\Im(y_t)|$ is among the γ -smallest values in $\{|\Im(y_t)|\}_{t=1}^m$ and the sign of $\Im(y_t)$ differs from $2\zeta_t - 1$. Furthermore, we shrink the imaginary part by a factor $\delta \in [-1, 1]$ to further limit the distortion:

$$y_t^{\text{wm}} = \begin{cases} \Re(y_t) - \mathbf{i}\delta \cdot \Im(y_t), & \text{if } \Im(y_t) \cdot (2\zeta_t - 1) < 0 \text{ and } |\Im(y_t)| \leq \text{Quantile}_\gamma(\{|\Im(y_t)|\}_{t=1}^m), \\ y_t, & \text{otherwise,} \end{cases} \quad (2)$$

and $y_{p-t}^{\text{wm}} = \overline{y_t^{\text{wm}}}$. When $\gamma = \delta = 1$, the soft variant (2) reduces to the hard sign flip (1); when $\gamma = 0$ and $\delta = -1$, it reduces to no watermarking. In practice, varying (γ, δ) enables flexible control over the trade-off between watermark strength and data fidelity. For example, one can tune (γ, δ) to maximize detectability under a given distortion budget by performing a lightweight grid search over synthetic samples. See Appendix G.2 for detailed computation overhead evaluation.

Step 3: Inverse steps to return to the original data domain. In the final step, we apply the inverse DFT to each modified \mathbf{y}^{wm} , collect the resulting vectors to form a matrix \mathbf{X}^{wm} , and then apply the inverse standardization followed by the inverse YJT to map it back into the original domain. For discrete features, we round values to the nearest valid entry. For example, a value of 0.4 for the “sex” entry would be rounded to 0 (female), while 0.6 would be rounded to 1 (male). For bounded features, we clip values to stay within the valid range. The full procedure is summarized in Algorithm 1. In Appendix G.1, we present an ablation study examining the impact of rounding and clipping on watermark detectability. In Section 4.5, We provide a case study to illustrate how TAB-DRW handles low-cardinality categorical variables, such as gender, in a conservative and adaptive manner that preserves their semantic validity.

Remark 1 (Related work). Modifying the DFT to embed watermarks has also been explored for diffusion models, such as Tree-Ring Watermarking [32]. However, this method typically applies deterministic, structured modifications (e.g., zeroing subregions), which are unsuitable for tabular data where each feature has distinct semantic meanings. In contrast, TAB-DRW performs fine-grained, row-wise perturbations guided by pseudorandom bits, preserving feature fidelity while enabling robust detection through a rank-based pseudorandom bit generation scheme.

Remark 2 (Column selection for watermarking). Since TAB-DRW is a lightweight post-editing watermark, model providers or dataset owners can flexibly choose any subset of columns to watermark based on their needs. For example, the watermark may be applied only to columns containing sensitive or high-value information that attackers are less likely to modify. In Section 4, we do not employ any specialized column selection strategy and exclude only columns with extreme distributions, which contribute little to the watermark signal and may cause scaling issues in a small number of rows even after YJT.

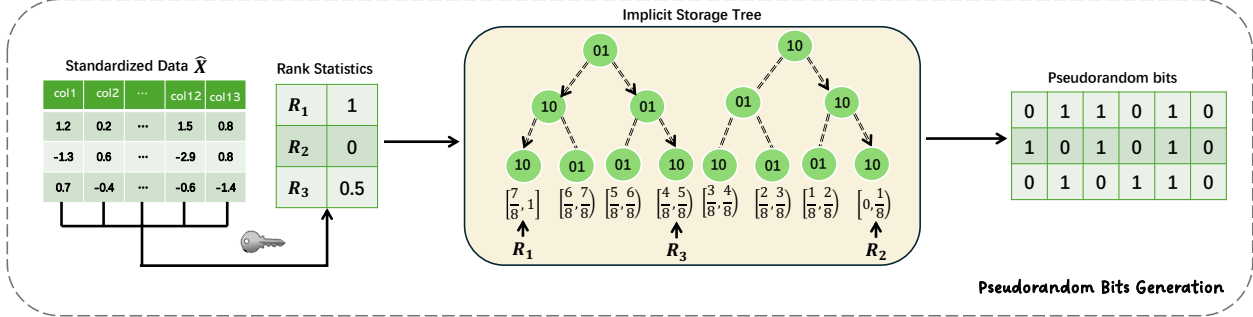


Figure 2: In the proposed pseudorandom bit generation scheme, bit sequence for each row is generated by mapping a row-wise rank statistic to a leaf node in a binary tree.

2.2 Watermark Detection

During detection, we can recover the pseudorandom bits using secret keys. Recall that TAB-DRW embeds watermark signals by flipping the imaginary signs in the frequency domain via the alignment with these pseudorandom bits. As a result, watermarked rows are expected to exhibit stronger alignment with the recovered pseudorandom bits. A natural detection strategy is to count the number of aligned entries in the suspect data under investigation: if the alignment is significantly higher than the expected without watermarking, we declare the data watermarked; otherwise, we do not. Statistically speaking, we solve the following hypothesis testing problem [11]:

$$H_0 : \text{The table is not watermarked} \quad \text{vs.} \quad H_1 : \text{The table is watermarked.}$$

Given a suspect tabular data $\mathbf{X} \in \mathbb{R}^{N \times p}$, we first apply **Step 1** of the watermark embedding procedure to obtain its frequency-domain representation $\mathbf{Y} = \{y_{i,j}\}_{i,j} \in \mathbb{C}^{N \times p}$, and denote the corresponding pseudorandom bits by $\{\zeta_{i,j}\}_{i,j}$. For each row i , we define the alignment count $T_i = \sum_{j=1}^m \mathbb{I}[\Im(y_{i,j}) \cdot (2\zeta_{i,j} - 1) > 0]$. We compute a one-sided Z-score to measure deviation from the expected alignment under H_0 :

$$Z = \frac{\frac{1}{N} \sum_{i=1}^N T_i - \mu_{\text{nwm}}}{\frac{\sigma_{\text{nwm}}}{\sqrt{N}}}, \quad (3)$$

where μ_{nwm} and σ_{nwm} denote the mean and standard deviation of T_i under H_0 . Given a critical value q_α for a significance level α , we reject H_0 and declare the table watermarked if $Z > q_\alpha$. In practice, we approximate μ_{nwm} , σ_{nwm} and q_α using Monte Carlo simulation.

2.3 Pseudorandom Bits Generation

The remaining issue is how to construct the pseudorandom bits used for embedding and detection. The design must satisfy two key requirements: 1) **robustness**, ensuring that recovered pseudorandom bits remain stable under post-processing attacks; and 2) **memory efficiency**, avoiding the impractical cost of explicitly storing pseudorandom bits for each generated table.

Informal description. To achieve the two goals, we propose a new pseudorandom bit generation scheme with two key components: 1) an implicit storage structure based on a binary tree, and 2) a retrieval mechanism using rank statistics. For each row of the standardized tabular data, we first use a secret key to select a subset \mathcal{I} of columns, then compute the sum of the entries in \mathcal{I} as a score for that row. This score determines the row's rank among all rows. We then normalize this rank to lie in $[0, 1]$. For example, if a row with m effective entries has rank $r = 1$ among $n = 3$ rows (i.e., the second-largest), its normalized rank is $\frac{r}{n-1} = 0.5$. We partition $[0, 1]$ into $2^{\lceil \frac{m}{2} \rceil}$ equal-sized bins and construct a binary tree of depth $\lceil \frac{m}{2} \rceil$, where each node is deterministically assigned a pseudorandom bit pair and each leaf corresponds to one bin. Each row's rank determines its bin, and the path from the root to the leaf encodes the pseudorandom bit sequence for that row. See Figure 2 for an illustration of the case $m = 6$ and Algorithm 3 for a formal description. Our pseudorandom bit generation scheme can be viewed as a variant of a Gray-code encoder; we provide more details on this connection in Appendix C.

Robustness of the pseudorandom bits. Our pseudorandom bit generation is robust against perturbations owing to two mechanisms. First, the subset \mathcal{I} of columns used for score computation is determined by the secret key. An

adversary without it cannot targetedly modify the specific entries that contribute to pseudorandom bit generation. Second, the sum-based rank statistic is highly stable, so small perturbations to a subset of columns (even those within \mathcal{I}) often do not change the bin to which the row belongs. As a result, the recovered pseudorandom bits typically remain correct. Even when the statistic shifts noticeably, it usually moves only to an adjacent bin. Our node-bit mapping policy ensures that adjacent bins differ by only a single bit pair, which limits the effect of such shifts on the recovered bit sequence. The tree-based structure enables deterministic computation of these mappings without requiring explicit storage.

3 Analysis on Distortion and Robustness

This section presents a theoretical analysis of the distortion and robustness properties of our watermarking scheme, offering insight into its foundational guarantees. The analysis is carried out on normalized tabular data after YJT and standardization, where each entry has zero mean and unit variance. This normalization reduces heterogeneity and facilitates theoretical analysis. Although the analysis assumes an idealized setting in the transformed domain without refitting the YJT parameters, all experiments use the full watermark embedding and detection pipeline as shown in Figure 1, consistent with realistic deployment. In Appendix D, we provide an empirical case study and additional evaluations showing that the effect of YJT refitting on both the data distribution and the watermark signal induced by sign-bit alignment is minimal, supporting the soundness of the idealized setting. The theoretical analysis is not intended to guarantee performance under all practical refinements of the pipeline, but rather to gain an intuition on why our method is fundamentally fidelity-preserving and robust. We also provide further analysis and complete proofs in Appendix E.

3.1 Watermark Distortion

Let $\mathbf{X} = \{x_{i,j}\}_{i,j} \in \mathbb{R}^{N \times p}$ be the tabular data where each column is centered and standardized, i.e., $\sum_{i=1}^N x_{i,j} = 0$ for all j and $\Sigma = \frac{1}{N} \mathbf{X}^\top \mathbf{X}$ with $\text{diag}(\Sigma) = \mathbb{I}_{p \times p}$. Recall that each row vector $\mathbf{x}_i := (x_{i,0}, \dots, x_{i,p-1}) \in \mathbb{R}^{1 \times p}$ is first mapped to the frequency domain via the DFT, then modified in some of imaginary components, and finally transformed back to the original domain. The following proposition characterizes the resulting entry-wise distortion—that is, the difference between the unwatermarked and watermarked table entries.

Proposition 1 (Entry-wise differences). *Let $S \subseteq \{1, \dots, m\}$ with $m = \lfloor \frac{p-1}{2} \rfloor$ denote the set of frequency coordinates whose imaginary signs are modified by our watermarking method. Let $\Delta x_{i,j} = x_{i,j}^{\text{wm}} - x_{i,j}$ denote the entry-wise difference. Then*

$$\Delta x_{i,j} = -\alpha \beta_j^\top \mathbf{x}_i, \quad \alpha = \frac{2(1+\delta)}{p},$$

where $\beta_j = (\beta_S(0, j), \dots, \beta_S(p-1, j))^\top$, and $\beta_S(n, j) = \sum_{k \in S} \sin\left(\frac{2\pi kn}{p}\right) \sin\left(\frac{2\pi kj}{p}\right)$.

Theorem 1 (Column-wise differences). *Our watermark affects column-wise quantities as follows:*

1. **Mean.** For each column j , the column mean is preserved: $\frac{1}{N} \sum_{i=1}^N \Delta x_{i,j} = 0$.

2. **Pearson correlation coefficients (PCC).** Let $r_{j\ell}$ and $r_{j\ell}^{\text{wm}}$ be the PCCs between columns j and ℓ before and after watermarking, respectively. Define $\Delta r_{j\ell} := r_{j\ell}^{\text{wm}} - r_{j\ell}$. Then,

$$\Delta r_{j\ell} = -\alpha ([\Sigma \beta_\ell]_j + [\Sigma \beta_j]_\ell) + \alpha^2 \beta_j^\top \Sigma \beta_\ell.$$

3. **Empirical distribution.** For each column j , let $\rho_j = \frac{1}{N} \sum_{i=1}^N \delta_{x_{i,j}}$ denote the empirical distribution of the unwatermarked entries, and let $\rho_j^{\text{wm}} = \frac{1}{N} \sum_{i=1}^N \delta_{x_{i,j}^{\text{wm}}}$ denote the corresponding distribution after watermarking. Let $\mathcal{W}_2(\cdot, \cdot)$ denote the Wasserstein-2 distance. Then,

$$\mathcal{W}_2(\rho_j, \rho_j^{\text{wm}}) \leq \alpha \sqrt{\beta_j^\top \Sigma \beta_j}.$$

The above theorem characterizes column-wise differences and highlights how the parameters (γ, δ) influence them. When $\delta = -1$, no imaginary components are changed, so $\alpha = 0$ and all three column-wise quantities remain unchanged. Similarly, when $\gamma = 0$, the selected frequency set S is empty, implying $\beta_j = \mathbf{0}$ for all j , and again, no distortion occurs. In contrast, when $(\gamma, \delta) \neq (0, -1)$, the bounds quantify the extent of distortion, revealing how the watermark parameters affect the data.

3.2 Watermark Robustness

In this section, we analyze the robustness of our watermarking scheme under Gaussian noise. We focus on the Z-score defined in (3). For unwatermarked data with independence assumption, the Z-score converges in distribution to standard normal distribution $\mathcal{N}(0, 1)$ (see Lemma 3 in the appendix). In contrast, for the watermarked table, the Z-score is significantly elevated. The following theorem shows that even after corruption with Gaussian noise, the expected Z-score remains high, indicating that our method embeds a strong and resilient watermark signal. In Appendix E.4, we extend the robustness analysis to a broader class of distributions by relaxing the Gaussian assumption in Theorem 2 to a sub-Gaussian setting. This setting accommodates non-Gaussian features with light-tailed distributions, including bounded or discrete categorical features.

Theorem 2 (Robustness). *We assume that unwatermarked tabular data $\mathbf{X} \in \mathbb{R}^{N \times p}$ has rows $\mathbf{x}_i \stackrel{\text{i.i.d.}}{\sim} \mathcal{N}(0, \Sigma)$, where $\Sigma \in \mathbb{R}^{p \times p}$ is positive-definite. Denote the smallest and largest eigenvalue of Σ by λ_{\min} and λ_{\max} , respectively. Define $Z(\gamma, \delta, \sigma)$ as the standard Z-score (as in (3)) computed on the Gaussian noise-corrupted table $\mathbf{X}_{\text{wm}} + \boldsymbol{\varepsilon}$, where $\mathbf{X}_{\text{wm}} \in \mathbb{R}^{N \times p}$ denote the table watermarked under soft hyperparameters (γ, δ) and $\boldsymbol{\varepsilon}_{i,j} \stackrel{\text{i.i.d.}}{\sim} \mathcal{N}(0, \sigma^2)$. Then, for any $\gamma \in [0, 1]$ and $\delta, \sigma > 0$,*

$$\mathbb{E}[Z(\gamma, \delta, \sigma)] \geq \sqrt{mN} \gamma \left[1 - \mathcal{I}(\sigma) - \mathcal{I}\left(\frac{\sigma}{\delta}\right) \right], \quad (4)$$

where $m = \lfloor \frac{p-1}{2} \rfloor$ and the function $\mathcal{I} : (0, \infty) \rightarrow \mathbb{R}$ is defined as

$$\mathcal{I}(s) := \frac{s}{\sqrt{s^2 + \lambda_{\min}}} \left[\Phi\left(\sqrt{1 + \frac{\lambda_{\min}}{s^2}}\right) - \frac{1}{2} \right] + \frac{s}{\sqrt{s^2 + \lambda_{\max}}} \left[1 - \Phi\left(\sqrt{1 + \frac{\lambda_{\max}}{s^2}}\right) \right] + \frac{1}{\sqrt{8\pi e}} \left[E_1\left(\frac{\lambda_{\min}}{2s^2}\right) - E_1\left(\frac{\lambda_{\max}}{2s^2}\right) \right].$$

with $\Phi(\cdot)$ denoting the standard normal CDF and $E_1(u) = \int_u^\infty \frac{e^{-t}}{t} dt$ the exponential integral.

Remark 3. We provide a numerical example to illustrate the guarantee in Theorem 2. When $(N, p) = (1000, 11)$ and $\Sigma = \mathbb{I}_{p \times p}$, the theoretical lower bound in the right-hand side of (4) is:

$$\mathbb{E}[Z(0.5, 0.5, \sigma)] \geq \begin{cases} 30.13, & \text{if } \sigma = 0.1, \\ 14.95, & \text{if } \sigma = 0.5, \\ 7.04, & \text{if } \sigma = 1.0. \end{cases}$$

Note that for a standard normal Z-score, the 0.99 quantile is 2.32. The above values are substantially larger, implying that the watermark signal remains significant even after noise corruption.

4 Experiments

In this section, we evaluate the performance of our proposed watermarking scheme on five benchmark tabular datasets along three dimensions: 1) data fidelity, 2) watermark detectability, and 3) robustness against post-processing and adaptive attacks. We also examine how the soft hyperparameters influence watermark strength, highlighting the inherent trade-off between data fidelity and detectability. We refer readers to Appendix G for additional empirical results, including comprehensive ablation studies in Appendix G.1, runtime analysis for watermark embedding and detection in Appendix G.2, extended robustness evaluations in Appendix G.3, and a practical evaluation of the privacy-enhanced TAB-DRW in real-world deployment settings in Appendix G.4.

4.1 Experimental Setup

Datasets. Experiments are conducted on five real-world tabular datasets with both continuous and discrete feature types: Adult [4], Magic [5], Shoppers [26], Default [38], and Drybean [16]. See details in Appendix F.1.

Baselines. We consider four baselines: two post-editing watermarking methods, GLW [11] and TabularMark [45], and two sampling-phase methods, TabWak* with valid bit mechanism [46] and MUSE [8]. We reproduce TabWak* using the official open-source code and implement other baselines according to the authors' specifications. To ensure fair comparison, We follow [46] to synthesize tabular data using TabSyn [40] with DDIM sampling. Further implementation details are provided in Appendix F.3 & F.4.

Metrics. We evaluate data fidelity using four metrics introduced in [40]: Marginal distribution (**Density**), inter-column correlation (**Corr**), classifier-two-sample-test score (**C2ST**), and machine learning efficiency (**MLE**). For watermark detection, we report two statistical metrics: the one-sided **Z-score** defined in (3), which quantifies the distributional shift of a pivotal statistic induced by watermarking, and **FPR / TPR**, the false and true positive rates under the critical value $q_\alpha = 6$, chosen to better distinguish detection performance. See Appendix F.2 for further details.

Table 2: Data fidelity and watermark detectability. No watermarking is denoted as “W/O”. Our proposed TAB-DRW is evaluated with the hyperparameter $(\gamma, \delta) = (0.5, 0.5)$. Best performances are shown in **bold**, and second-best are underlined.

Datasets	Method	Fidelity Metric				Z-score		FPR / TPR	
		Density \uparrow	Corr \uparrow	C2ST \uparrow	MLE \uparrow	1k rows \uparrow	5k rows \uparrow	1k rows \uparrow	5k rows \uparrow
Adult	W/O	0.922 \pm 0.001	0.872 \pm 0.001	0.611 \pm 0.004	0.824 \pm 0.005	—	—	—	—
	GLW	0.912 \pm 0.002	0.871 \pm 0.002	0.604 \pm 0.015	0.821 \pm 0.017	7.293 \pm 0.96	16.54 \pm 1.05	0.00/0.91	0.00/1.00
	MUSE	<u>0.921</u> \pm 0.001	0.877 \pm <u>0.003</u>	0.599 \pm 0.007	<u>0.823</u> \pm 0.005	6.712 \pm 0.89	14.81 \pm 1.23	0.00/0.78	0.00/1.00
	TabWak*	0.912 \pm 0.002	0.863 \pm 0.004	0.604 \pm 0.009	0.793 \pm 0.009	6.796 \pm 1.03	15.67 \pm 0.97	0.00/0.78	0.00/1.00
	TabularMark	0.922 \pm <u>0.001</u>	0.872 \pm 0.001	0.598 \pm 0.006	0.823 \pm <u>0.003</u>	9.674 \pm 3.00	22.53 \pm 3.05	0.00/0.89	0.00/1.00
	TAB-DRW	0.915 \pm 0.005	0.864 \pm 0.004	0.604 \pm 0.008	0.816 \pm 0.009	12.81 \pm <u>1.17</u>	29.55 \pm <u>1.12</u>	0.00/1.00	0.00/1.00
Magic	W/O	0.917 \pm 0.001	0.945 \pm 0.003	0.672 \pm 0.004	0.823 \pm 0.007	—	—	—	—
	GLW	0.915 \pm 0.001	0.944 \pm <u>0.002</u>	0.669 \pm 0.013	0.816 \pm 0.006	77.05 \pm <u>0.55</u>	172.2 \pm <u>0.51</u>	0.00/1.00	0.00/1.00
	MUSE	0.912 \pm 0.002	0.943 \pm 0.006	0.672 \pm 0.008	<u>0.824</u> \pm 0.017	15.84 \pm 0.86	35.31 \pm 0.70	0.00/1.00	0.00/1.00
	TabWak*	0.912 \pm 0.007	0.921 \pm 0.003	0.671 \pm 0.006	0.827 \pm <u>0.029</u>	8.608 \pm 0.98	19.83 \pm 1.01	0.00/1.00	0.00/1.00
	TabularMark	0.917 \pm <u>0.001</u>	0.943 \pm 0.003	0.674 \pm 0.005	0.822 \pm 0.009	9.666 \pm 2.82	22.02 \pm 3.62	0.00/0.90	0.00/1.00
	TAB-DRW	0.917 \pm 0.005	0.937 \pm 0.003	0.676 \pm <u>0.009</u>	0.818 \pm 0.014	27.34 \pm 0.93	61.42 \pm 1.02	0.00/1.00	0.00/1.00
Shoppers	W/O	0.919 \pm 0.002	0.910 \pm 0.001	0.704 \pm 0.005	0.902 \pm 0.012	—	—	—	—
	GLW	0.903 \pm 0.001	0.908 \pm <u>0.001</u>	0.706 \pm 0.018	0.893 \pm 0.009	17.84 \pm <u>1.12</u>	39.08 \pm <u>1.05</u>	0.00/1.00	0.00/1.00
	MUSE	0.911 \pm 0.001	0.908 \pm 0.002	0.710 \pm 0.009	0.895 \pm 0.012	12.80 \pm 0.88	28.83 \pm 0.87	0.00/1.00	0.00/1.00
	TabWak*	0.916 \pm <u>0.009</u>	0.906 \pm 0.001	0.674 \pm 0.021	0.905 \pm <u>0.047</u>	4.071 \pm 1.06	10.38 \pm 1.02	0.00/0.04	0.00/1.00
	TabularMark	0.914 \pm 0.003	0.908 \pm 0.001	0.704 \pm 0.005	0.897 \pm 0.018	10.28 \pm 3.24	22.94 \pm 3.36	0.00/0.91	0.00/1.00
	TAB-DRW	0.909 \pm 0.006	0.902 \pm 0.003	0.712 \pm <u>0.013</u>	0.891 \pm 0.014	18.18 \pm <u>1.28</u>	40.74 \pm <u>1.26</u>	0.00/1.00	0.00/1.00
Default	W/O	0.930 \pm 0.001	0.907 \pm 0.001	0.717 \pm 0.003	0.797 \pm 0.009	—	—	—	—
	GLW	0.926 \pm 0.002	0.906 \pm 0.003	0.710 \pm 0.027	0.787 \pm 0.011	12.10 \pm 1.09	27.08 \pm 0.99	0.00/1.00	0.00/1.00
	MUSE	0.928 \pm 0.001	0.907 \pm 0.002	0.714 \pm 0.008	0.790 \pm 0.007	15.50 \pm <u>0.97</u>	34.42 \pm <u>0.95</u>	0.00/1.00	0.00/1.00
	TabWak*	0.934 \pm <u>0.011</u>	0.912 \pm <u>0.014</u>	0.723 \pm <u>0.048</u>	0.775 \pm 0.009	10.49 \pm 1.03	23.60 \pm 1.00	0.00/1.00	0.00/1.00
	TabularMark	0.927 \pm 0.005	0.902 \pm 0.006	0.718 \pm 0.007	0.796 \pm <u>0.009</u>	9.526 \pm 2.91	23.94 \pm 3.18	0.00/0.89	0.00/1.00
	TAB-DRW	0.929 \pm 0.010	0.907 \pm 0.011	0.717 \pm 0.018	0.791 \pm 0.013	15.98 \pm <u>0.92</u>	35.84 \pm <u>0.91</u>	0.00/1.00	0.00/1.00
Drybean	W/O	0.932 \pm 0.001	0.935 \pm 0.001	0.640 \pm 0.003	0.878 \pm 0.009	—	—	—	—
	GLW	0.929 \pm 0.002	0.933 \pm 0.004	0.637 \pm 0.017	0.872 \pm 0.013	55.14 \pm <u>0.66</u>	123.3 \pm <u>0.68</u>	0.00/1.00	0.00/1.00
	MUSE	0.930 \pm 0.003	0.934 \pm 0.005	0.649 \pm 0.011	0.878 \pm 0.014	14.14 \pm 1.03	31.43 \pm 0.91	0.00/1.00	0.00/1.00
	TabWak*	0.924 \pm 0.014	0.925 \pm 0.008	0.659 \pm <u>0.032</u>	0.875 \pm 0.015	7.999 \pm 0.92	17.80 \pm 0.97	0.00/0.99	0.00/1.00
	TabularMark	0.932 \pm <u>0.002</u>	0.935 \pm <u>0.001</u>	0.641 \pm 0.005	0.878 \pm 0.011	7.760 \pm 3.14	17.28 \pm 2.73	0.00/0.71	0.00/1.00
	TAB-DRW	0.931 \pm 0.013	0.928 \pm 0.007	0.655 \pm 0.029	0.880 \pm <u>0.019</u>	38.03 \pm 1.03	85.05 \pm 0.67	0.00/1.00	0.00/1.00

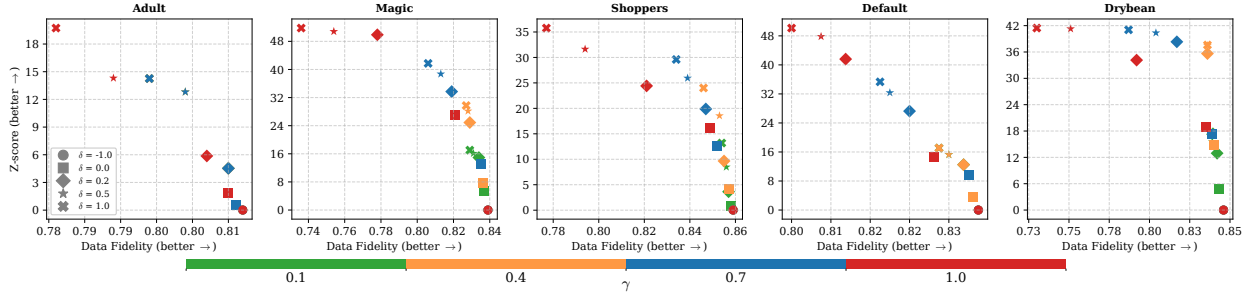


Figure 3: Trade-off between average Z-score on 1K-rows tables and data fidelity under varying (γ, δ) .

4.2 Data Fidelity vs. Watermark Detectability

To evaluate data fidelity, we generate synthetic tabular datasets with the same number of rows as the original for each of the five datasets. For watermark detectability, we compute both Z-scores and FPR/TPR using two batch sizes: 1k and 5k rows. Table 2 reports the mean and standard deviation of each fidelity metric over 10 independent trials, and each detectability metric over 100 trials.

On one hand, our watermarking scheme introduces minimal distortion. Across all datasets, its fidelity scores closely match those of the unwatermarked data (degrading by no more than 0.01) and are comparable to existing baselines. While TabWak* and TabularMark often achieve the highest fidelity, our method with $(\gamma, \delta) = (0.5, 0.5)$ performs similarly well. Overall, all baseline methods yield comparable fidelity scores, indicating that our approach preserves data quality on par with prior work. On the other hand, in terms of watermark detectability, our method achieves the highest Z-scores on the Adult, Shoppers, and Default datasets. GLW performs best on Magic and Drybean, likely due

Table 3: Watermark robustness against attacks. Average Z-score on 5k rows under ten post-processing attacks. Each value is obtained by repeating the attacks 100 times (10 times for “TabWak**”) and averaging the results. Our proposed TAB-DRW is evaluated with the hyperparameter $(\gamma, \delta) = (0.5, 0.5)$. Best performances are shown in **bold**, and second-best are underlined.

Datasets	Method	Attacks									
		Row Del.	Col Del.	Cell Del.	G-Noise	C-Noise	A-Noise	Truncation	Quantization	Resample	Shuffle
Adult	GLW	15.69	14.55	14.88	0.00	<u>16.54</u>	7.26	<u>16.54</u>	8.63	16.89	16.54
	MUSE	14.00	6.26	9.16	<u>12.83</u>	10.91	4.53	14.81	10.96	<u>20.15</u>	14.81
	TabWak*	14.98	11.32	11.08	0.91	15.67	<u>14.50</u>	5.09	<u>11.27</u>	16.37	15.67
	TabularMark	21.65	<u>15.56</u>	<u>16.42</u>	2.83	6.90	1.29	2.72	0.00	4.62	<u>17.44</u>
Magic	TAB-DRW	27.98	17.78	20.46	20.36	24.59	23.72	29.55	20.95	28.15	29.55
	GLW	163.33	140.15	154.89	0.03	172.20	1.09	14.71	47.28	170.81	172.20
	MUSE	33.55	7.16	17.91	15.99	34.33	9.09	<u>20.06</u>	14.54	33.59	35.31
	TabWak*	18.92	13.18	16.33	<u>17.99</u>	19.76	<u>13.86</u>	16.87	16.50	17.62	19.76
Shoppers	TabularMark	20.65	12.05	13.80	0.00	20.05	0.35	13.66	0.65	21.04	15.26
	TAB-DRW	58.28	17.45	35.78	46.18	54.48	40.72	52.62	45.14	37.61	61.42
	GLW	36.82	36.02	36.15	0.00	39.08	1.11	24.61	7.20	31.92	39.08
	MUSE	27.34	11.37	15.34	<u>23.56</u>	21.58	<u>16.74</u>	23.14	<u>19.84</u>	28.63	28.83
Default	TabWak*	9.55	3.33	4.68	0.02	10.47	5.08	9.05	7.82	10.71	10.47
	TabularMark	15.48	11.17	14.66	1.46	18.43	0.13	11.40	3.02	18.23	18.62
	TAB-DRW	38.43	19.35	22.99	39.66	36.26	20.66	30.28	32.46	29.28	40.74
	GLW	25.67	<u>24.59</u>	23.88	0.00	<u>27.08</u>	9.08	27.08	11.94	15.82	27.08
Drybean	MUSE	<u>32.75</u>	11.38	13.11	19.81	24.25	4.98	<u>34.42</u>	11.17	36.60	<u>34.42</u>
	TabWak*	22.91	18.36	18.96	<u>22.95</u>	23.70	21.79	22.80	<u>19.83</u>	31.49	23.70
	TabularMark	21.66	15.79	12.46	0.00	21.53	0.23	12.36	0.86	20.94	23.33
	TAB-DRW	33.92	25.03	22.56	30.03	32.22	21.55	35.84	21.93	32.36	35.84
Drybean	GLW	116.96	112.05	110.89	0.00	123.28	13.29	28.02	29.37	123.68	123.28
	MUSE	29.78	7.76	12.32	6.22	29.56	6.28	10.43	1.89	31.19	31.43
	TabWak*	17.16	0.00	2.86	<u>14.11</u>	17.53	<u>13.59</u>	16.80	6.56	15.38	17.53
	TabularMark	13.79	7.18	9.55	0.00	13.56	0.00	7.57	0.66	12.88	10.46
	TAB-DRW	80.62	42.82	50.99	31.12	80.43	58.50	42.14	61.23	68.69	85.05

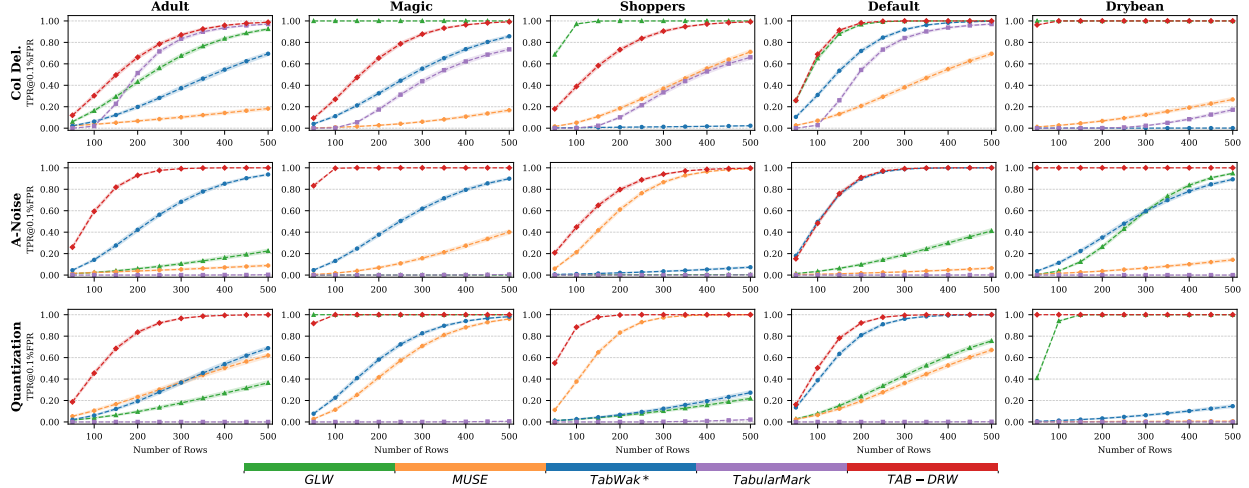


Figure 4: TPR@0.1%FPR versus row count under three representative attacks. Dashed lines show the bootstrap mean estimate (500 resamples), and shaded regions indicate the 90% confidence interval.

to the predominance of continuous attributes. Most methods—including ours—successfully control false positive rates and show nontrivial true positive rates under the critical threshold $q_\alpha = 6$, demonstrating reliable detectability. The results in Figure 3 also reveal a trade-off between data fidelity and watermark strength for our method. Increasing both γ and δ enhances the Z-score, but also increases distortion. This trade-off is inherent to post-editing watermarking: stronger signals inevitably introduce more distortion. Similar additional results on TabSyn with score-based diffusion process and two other tabular generators, together with ablation study on TAB-DRW components, are presented in Appendix G.1.

Table 4: Robustness of TAB-DRW against adversarial row deletion attacks of varying strength. Z-scores are computed on tables with 5k rows and averaged over 100 independent trials.

Datasets	No-attack	Adv. Row Del.@0.1	Adv. Row Del.@0.2	Adv. Row Del.@0.5
Adult	29.12 ± 1.12	28.55 ± 1.44	26.35 ± 2.61	18.79 ± 4.47
Magic	61.42 ± 1.02	56.71 ± 2.98	49.36 ± 5.77	28.41 ± 7.28
Shoppers	40.74 ± 1.26	36.47 ± 2.62	30.40 ± 3.71	17.12 ± 4.18
Default	35.84 ± 0.91	31.91 ± 1.90	27.13 ± 3.23	15.36 ± 4.54
Drybean	85.05 ± 0.67	79.27 ± 2.67	71.67 ± 5.04	52.39 ± 9.99

Table 5: Robustness of TAB-DRW against rewatermarking attacks of varying strength. Fidelity is averaged over four metrics across 10 independent trials, and the Z-scores are computed on tables with 5k rows and averaged over 100 independent trials. “Rewatermarking@ n ” denotes rewatermarking the table using n randomly sampled keys.

Datasets	No-attack		Rewatermarking@1		Rewatermarking@3		Rewatermarking@10	
	Fidelity	Z-score	Fidelity	Z-score	Fidelity	Z-score	Fidelity	Z-score
Adult	0.799 ± 0.006	29.55 ± 1.12	0.787 ± 0.008	23.66 ± 1.17	0.772 ± 0.006	16.26 ± 1.09	0.766 ± 0.009	17.26 ± 1.34
Magic	0.837 ± 0.008	61.42 ± 1.02	0.822 ± 0.008	53.23 ± 0.91	0.813 ± 0.007	34.32 ± 0.93	0.799 ± 0.008	29.17 ± 1.00
Shoppers	0.854 ± 0.009	40.74 ± 1.26	0.847 ± 0.008	31.97 ± 1.15	0.829 ± 0.009	20.14 ± 1.09	0.813 ± 0.008	16.67 ± 1.09
Default	0.836 ± 0.013	35.84 ± 0.91	0.827 ± 0.011	32.85 ± 1.00	0.811 ± 0.013	19.40 ± 1.07	0.809 ± 0.010	26.28 ± 1.18
Drybean	0.849 ± 0.017	85.05 ± 0.67	0.832 ± 0.017	44.79 ± 0.81	0.801 ± 0.017	29.47 ± 0.83	0.806 ± 0.014	33.77 ± 0.95

4.3 Robustness against Post-Processing Attacks

We next evaluate the robustness of watermarking methods against ten post-processing attacks, which can be grouped into four categories: 1) deletion attacks, which remove or replace information at different granularities (**Row Del.**, **Col Del.**, **Cell Del.**); 2) noise attacks, which perturb numerical or categorical values with Gaussian, categorical, or adaptive noise (**G-Noise**, **C-Noise**, **A-Noise**); 3) discretization attacks, which reduce numeric precision through truncation or quantization (**Truncation**, **Quantization**); and 4) structural attacks, which alter table structure by resampling label distributions or randomly shuffling rows (**Resample**, **Shuffle**). Detailed definition and implementations of the attacks are provided in Appendix F.5.

Table 3 reports the average one-sided Z -score over 5k rows. Our watermarking method consistently demonstrates superior robustness across all attack types and datasets, ranking either first or second. In contrast, GLW and TabularMark remain resilient to deletion and structural attacks but often fail under noise and discretization. TabWak* and MUSE exhibit some robustness to noise and discretization on certain datasets, but they are vulnerable to deletion attacks due to their reliance on complete column information. Figure 4 shows TPR@0.1%FPR versus the number of rows under three representative and strong attacks. Among ten out of fifteen cases, our method reaches 1.0 TPR@0.1%FPR using only 300 rows, with the remaining five cases requiring fewer than 500 rows. In contrast, baseline methods often suffer reduced true positive rates or completely lose detectability under these conditions.

4.4 Robustness against Adaptive Attacks

In this section, we implemented two adaptive attacks. In both cases, we consider adversaries who fully understand our pipeline, including the privacy-enhanced version (cf. Appendix B) for real-world deployment, but do not know the secret key.

The first attack, **Adaptive Row Deletion**, aims to corrupt the row ranking and thus impair rank-based bit retrieval. The attacker generates a random key, computes the normalized rank of each row (following lines 3–6 of Algorithm 3), and then deletes a block of rows whose ranks form a contiguous interval. For example, under strength 0.1, the adversary removes rows whose normalized ranks lie within a randomly selected interval of length 0.1 in $[0, 1]$. This manipulation disrupts the ranking structure significantly more than random row deletion.

The second attack, **Rewatermarking**, targets to erase sign-bit alignment in the frequency domain. It exploits two properties of our privacy-enhanced TAB-DRW: first, its strong fidelity-preserving performance, and second, the fact that a watermark embedded with one key cannot be detected using another. An informed adversary can therefore repeatedly rewatermark the table with multiple different keys, aiming to perturb the original alignment and render the watermark undetectable to the original detection key.

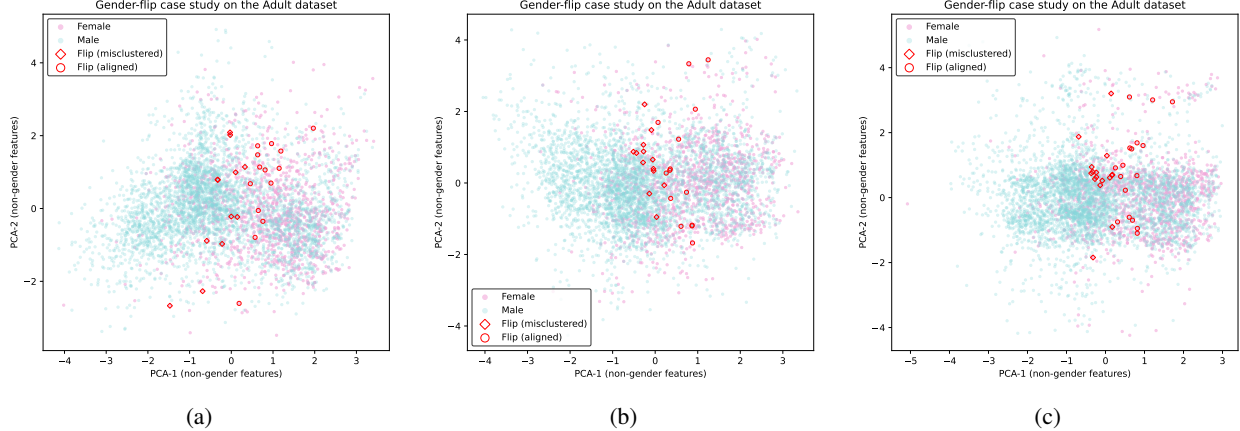


Figure 5: Visualization of the gender-flipping case study on the Adult dataset. Each subfigure corresponds to a synthetic 5K-row table pair (watermarked vs. unwatermarked). “Flip (misclustered)” denotes samples whose original “gender” label conflicts with their cluster label and subsequently flips after watermarking. “Flip (aligned)” denotes samples whose original “gender” label matches the cluster label but still flips after watermarking. In subfigure (a), 26 out of 5K samples exhibit a gender flip (46.2% misclustered); their mean distance to the cluster boundary is 0.31, compared with 0.78 for the remaining samples. In subfigure (b), 27 out of 5K samples exhibit a gender flip (48.1% misclustered); their mean distance to the cluster boundary is 0.26, compared with 0.75 for the remaining samples. In subfigure (c), 33 out of 5K samples exhibit a gender flip (48.5% misclustered); their mean distance to the cluster boundary is 0.29, compared with 0.77 for the remaining samples.

The results in Table 4 show that TAB-DRW remains highly detectable even under substantial adaptive row-deletion attacks. Although detectability decreases slightly compared with random row deletion, the use of a secret key and the stable tree-based bit-storage enables TAB-DRW to be resilient to these attacks specifically crafted to disrupt the row-ranking process. From the results in Table 5, we observe that TAB-DRW remains highly detectable even after ten rounds of rewatermarking, at which point the fidelity of the tabular data has already been noticeably degraded. These findings demonstrate that, without knowledge of the key used in Algorithm 2 and 3, an attacker—despite understanding the TAB-DRW pipeline—cannot substantially disrupt the sign-bit alignment while preserving data fidelity.

4.5 A Case Study on Low-Cardinality Categorical Variable

TAB-DRW handles low-cardinality categorical variables such as “gender” in a conservative and adaptive manner. The row-wise DFT maps each standardized sample into a frequency-domain representation whose components are linear combinations of all entries in the row. As a result, watermark embedding via imaginary sign-bit alignment operates on this joint representation rather than on any single attribute. Whether a sample’s “gender” value remains unchanged or flips therefore depends on how the sample is positioned relative to the distribution of its other features. When we cluster unwatermarked samples using all non-“gender” variables, the samples whose “gender” will flip after watermarking always lie near cluster boundaries or appear misclustered. In this sense, the flipped “gender” value remains semantically compatible with the rest features of the sample.

We conduct a case study on the **Adult** dataset and focus on the flipping of “gender” variable. Specifically, we randomly select three pairs of 5K-row tables (watermarked vs. unwatermarked). After applying the YJT to standardize feature scales, we performed PCA on the non-“gender” variables and retained the first two principal components for each sample. Based on these two principal components, we applied k -means clustering with $k = 2$, yielding two clusters that correspond to “female-like” and “male-like” profiles. We then examined the samples whose “gender” flips after watermarking, dividing them into two groups: those whose original “gender” label align with the cluster label and those that are misclustered. The visualization results in Figure 5 reveal several findings:

1. Flips in low-cardinality categorical variables are rare under TAB-DRW. In a 5K-row table, we typically observe only around 30 such cases.
2. Nearly half of the flipped samples are misclustered before watermarking, suggesting that the watermark embedding improves rather than disrupts their semantic coherence.

3. Among the remaining aligned samples that flip, we find that they tend to lie close to the cluster boundary. Across the three table examples, their average distance to the boundary is 0.29, compared with 0.77 for the other samples. This indicates that even when a flip occurs, the resulting “gender” value remains semantically meaningful.

5 Conclusion

In this paper, we present TAB-DRW, a lightweight and robust post-editing watermarking scheme for tabular data. TAB-DRW normalizes heterogeneous features via the Yeo–Johnson transformation and standardization, and embeds watermarks by adjusting the imaginary parts of adaptively selected frequency-domain entries. It achieves strong detectability and high fidelity across mixed-type datasets—without relying on large diffusion models or explicitly storing unwatermarked data. Our proposed rank-based pseudorandom bit generation method enables efficient row-wise retrieval via robust rank statistics, further enhancing resilience to post-processing and adaptive attacks. We provide theoretical analysis of watermark distortion and robustness against noise perturbations; and validate our approach on five benchmark datasets, demonstrating broad applicability, high fidelity, strong detectability, and great robustness. We believe that TAB-DRW offers a solid foundation for advancing secure data sharing and the development of privacy-preserving generative AI.

References

- [1] Scott Aaronson. Watermarking of large language models. <https://simons.berkeley.edu/talks/scott-aaronson-ut-austin-openai-2023-08-17>, 2023.
- [2] Samuel A Assefa, Danial Dervovic, Mahmoud Mahfouz, Robert E Tillman, Prashant Reddy, and Manuela Veloso. Generating synthetic data in finance: Opportunities, challenges and pitfalls. In *Proceedings of the First ACM International Conference on AI in Finance*, pages 1–8, 2020.
- [3] André Bauer, Simon Trapp, Michael Stenger, Robert Leppich, Samuel Kounev, Mark Leznik, Kyle Chard, and Ian Foster. Comprehensive exploration of synthetic data generation: A survey. *arXiv preprint arXiv:2401.02524*, 2024.
- [4] Barry Becker and Ronny Kohavi. Adult. UCI Machine Learning Repository, 1996. DOI: <https://doi.org/10.24432/C5XW20>.
- [5] R. Bock. MAGIC Gamma Telescope. UCI Machine Learning Repository, 2004. DOI: <https://doi.org/10.24432/C52C8B>.
- [6] Vadim Borisov, Tobias Leemann, Kathrin Seßler, Johannes Haug, Martin Pawelczyk, and Gjergji Kasneci. Deep neural networks and tabular data: A survey. *IEEE transactions on neural networks and learning systems*, 2022.
- [7] Tianqi Chen and Carlos Guestrin. XGBoost: A scalable tree boosting system. In *Proceedings of the 22nd ACM SIGKDD International Conference on Knowledge Discovery and Data Mining*, page 785–794, 2016.
- [8] Liancheng Fang, Aiwei Liu, Henry Peng Zou, Yankai Chen, Hengrui Zhang, Zhongfen Deng, and Philip S Yu. MUSE: Model-Agnostic Tabular Watermarking via Multi-Sample Selection. *arXiv preprint arXiv:2505.24267*, 2025.
- [9] Manbir Gulati and Paul Roysdon. TabMT: Generating tabular data with masked transformers. In *Advances in Neural Information Processing Systems*, 2024.
- [10] Xu Guo and Yiqiang Chen. Generative AI for synthetic data generation: Methods, challenges and the future. *arXiv preprint arXiv:2403.04190*, 2024.
- [11] Hengzhi He, Peiyu Yu, Junpeng Ren, Ying Nian Wu, and Guang Cheng. Watermarking generative tabular data. *arXiv preprint arXiv:2405.14018*, 2024.
- [12] Baizhou Huang and Xiaojun Wan. WaterPool: A language model watermark mitigating trade-offs among imperceptibility, efficacy and robustness. In *Proceedings of the 2025 Conference of the Nations of the Americas Chapter of the Association for Computational Linguistics: Human Language Technologies (Volume 1: Long Papers)*, pages 4156–4182. Association for Computational Linguistics, April 2025.
- [13] Jayoung Kim, Chaejeong Lee, and Noseong Park. Stasy: Score-based tabular data synthesis. In *International Conference on Learning Representations*, 2023.
- [14] Diederik P Kingma and Max Welling. Auto-encoding variational bayes. In *International Conference on Learning Representations*, 2014.
- [15] John Kirchenbauer, Jonas Geiping, Yuxin Wen, Jonathan Katz, Ian Miers, and Tom Goldstein. A watermark for large language models. In *International Conference on Machine Learning*, pages 17061–17084. PMLR, 2023.
- [16] Murat Koklu and İlker Ali Özkan. Multiclass classification of dry beans using computer vision and machine learning techniques. *Comput. Electron. Agric.*, 174:105507, 2020.
- [17] Akim Kotelnikov, Dmitry Baranchuk, Ivan Rubachev, and Artem Babenko. TabDDPM: Modelling tabular data with diffusion models. In *International Conference on Machine Learning*, pages 17564–17579. PMLR, 2023.
- [18] Rohith Kuditipudi, John Thickstun, Tatsunori Hashimoto, and Percy Liang. Robust distortion-free watermarks for language models. *Transactions on Machine Learning Research*, 2024.
- [19] Xiang Li, Feng Ruan, Huiyuan Wang, Qi Long, and Weijie J Su. A statistical framework of watermarks for large language models: Pivot, detection efficiency and optimal rules. *The Annals of Statistics*, 53(1):322–351, 2025.
- [20] Ruibo Liu, Jerry Wei, Fangyu Liu, Chenglei Si, Yanzhe Zhang, Jinmeng Rao, Steven Zheng, Daiyi Peng, Diyi Yang, Denny Zhou, and Andrew M. Dai. Best practices and lessons learned on synthetic data. In *First Conference on Language Modeling*, 2024.
- [21] Tennison Liu, Zhaozhi Qian, Jeroen Berrevoets, and Mihaela van der Schaar. GOGGLE: Generative modelling for tabular data by learning relational structure. In *International Conference on Learning Representations*, 2023.
- [22] Nils Lukas and Florian Kerschbaum. PTW: Pivotal tuning watermarking for pre-trained image generators. In *32nd USENIX Security Symposium (USENIX Security 23)*, pages 2241–2258, 2023.

- [23] Alan V Oppenheim. *Discrete-time signal processing*. Pearson Education India, 1999.
- [24] Christine I Podilchuk and Edward J Delp. Digital watermarking: Algorithms and applications. *IEEE signal processing Magazine*, 18(4):33–46, 2001.
- [25] Zhaozhi Qian, Thomas Callender, Bogdan Cebere, Sam M Janes, Neal Navani, and Mihaela van der Schaar. Synthetic data for privacy-preserving clinical risk prediction. *Scientific Reports*, 14(1):25676, 2024.
- [26] C. Sakar and Yomi Castro. Online Shoppers Purchasing Intention Dataset. UCI Machine Learning Repository, 2018. DOI: <https://doi.org/10.24432/C5F88Q>.
- [27] SciPy Developers. `scipy.stats.yeojohnson` — scipy documentation. <https://docs.scipy.org/doc/scipy/reference/generated/scipy.stats.yeojohnson.html>, 2025.
- [28] Jiaming Song, Chenlin Meng, and Stefano Ermon. Denoising diffusion implicit models. In *International Conference on Learning Representations*, 2021.
- [29] Roman Vershynin. *High-dimensional probability: An introduction with applications in data science*, volume 47. Cambridge university press, 2018.
- [30] Nikhil Vyas, Sham M Kakade, and Boaz Barak. On provable copyright protection for generative models. In *International Conference on Machine Learning*, pages 35277–35299. PMLR, 2023.
- [31] Alex X. Wang and Binh P. Nguyen. TTVAE: Transformer-based generative modeling for tabular data generation. *Artificial Intelligence*, 340:104292, 2025.
- [32] Yuxin Wen, John Kirchenbauer, Jonas Geiping, and Tom Goldstein. Tree-rings watermarks: Invisible fingerprints for diffusion images. In *Advances in Neural Information Processing Systems*, pages 58047–58063, 2023.
- [33] Bram Wouters. Optimizing watermarks for large language models. In *International Conference on Machine Learning*, pages 53251–53269. PMLR, 2024.
- [34] Yihan Wu, Zhengmian Hu, Hongyang Zhang, and Heng Huang. A resilient and accessible distribution-preserving watermark for large language models. In *International Conference on Machine Learning*. PMLR, 2024.
- [35] Yangxinyu Xie, Xiang Li, Tanwi Mallick, Weijie Su, and Ruixun Zhang. Debiasing watermarks for large language models via maximal coupling. *Journal of the American Statistical Association*, (just-accepted):1–21, 2025.
- [36] Lei Xu, Maria Skoularidou, Alfredo Cuesta-Infante, and Kalyan Veeramachaneni. Modeling tabular data using conditional GAN. In *Advances in Neural Information Processing Systems*, 2019.
- [37] Zijin Yang, Kai Zeng, Kejiang Chen, Han Fang, Weiming Zhang, and Nenghai Yu. Gaussian shading: Provable performance-lossless image watermarking for diffusion models. In *Proceedings of the IEEE/CVF Conference on Computer Vision and Pattern Recognition*, pages 12162–12171, 2024.
- [38] I-Cheng Yeh. Default of Credit Card Clients. UCI Machine Learning Repository, 2009. DOI: <https://doi.org/10.24432/C55S3H>.
- [39] In-Kwon Yeo and Richard A Johnson. A new family of power transformations to improve normality or symmetry. *Biometrika*, 87(4):954–959, 2000.
- [40] Hengrui Zhang, Jian Zhang, Balasubramaniam Srinivasan, Zhengyuan Shen, Xiao Qin, Chris Faloutsos, Huzefa Rangwala, and George Karypis. Mixed-type tabular data synthesis with score-based diffusion in latent space. In *International Conference on Learning Representations*, 2024.
- [41] Lijun Zhang, Xiao Liu, Antoni Viros Martin, Cindy Xiong Bearfield, Yuriy Brun, and Hui Guan. Attack-resilient image watermarking using stable diffusion. In *Advances in Neural Information Processing Systems*, 2024.
- [42] Yishuo Zhang, Nayyar A Zaidi, Jiahui Zhou, and Gang Li. GANBLR: A tabular data generation model. In *2021 IEEE International Conference on Data Mining*, pages 181–190. IEEE, 2021.
- [43] Xuandong Zhao, Prabhanjan Vijendra Ananth, Lei Li, and Yu-Xiang Wang. Provable robust watermarking for AI-generated text. In *International Conference on Learning Representations*, 2024.
- [44] Zilong Zhao, Aditya Kunar, Robert Birke, and Lydia Y Chen. CYAB-GAN: Effective table data synthesizing. In *Asian Conference on Machine Learning*, pages 97–112. PMLR, 2021.
- [45] Yihao Zheng, Haocheng Xia, Junyuan Pang, Jinfei Liu, Kui Ren, Lingyang Chu, Yang Cao, and Li Xiong. TabularMark: Watermarking tabular datasets for machine learning. In *Proceedings of the 2024 on ACM SIGSAC Conference on Computer and Communications Security*, pages 3570–3584, 2024.
- [46] Chaoyi Zhu, Jiayi Tang, Jeroen M Galjaard, Pin-Yu Chen, Robert Birke, Cornelis Bos, Lydia Y Chen, et al. TabWak: A watermark for tabular diffusion models. In *International Conference on Learning Representations*, 2025.

Contents

1	Introduction	1
2	Method	3
2.1	Watermark Embedding	3
2.2	Watermark Detection	5
2.3	Pseudorandom Bits Generation	5
3	Analysis on Distortion and Robustness	6
3.1	Watermark Distortion	6
3.2	Watermark Robustness	7
4	Experiments	7
4.1	Experimental Setup	7
4.2	Data Fidelity vs. Watermark Detectability	8
4.3	Robustness against Post-Processing Attacks	10
4.4	Robustness against Adaptive Attacks	10
4.5	A Case Study on Low-Cardinality Categorical Variable	11
5	Conclusion	12
A	Related Works	17
B	Privacy-Enhanced TAB-DRW	17
C	Missing Details from Section 2	18
D	Missing Details from Section 3	19
E	Theoretical Analysis and Proofs	21
E.1	Proof of Proposition 1	21
E.2	Proof of Theorem 1	21
E.3	Proof of Theorem 2	22
E.4	Further Analysis on Robustness	25
F	Experimental Details	27
F.1	Datasets	27
F.2	Metrics	28
F.3	Implementation Details for Data Generator	29
F.4	Implementation Details for Watermarking	29
F.5	Implementation Details for Tabular Attacks	30
G	Additional Results and Analysis	31

G.1	Ablation Study	31
G.2	Runtime Evaluation	34
G.3	Additional Robustness Evaluation	36
G.4	Privacy-Enhanced TAB-DRW Evaluation	37
H	Discussion and Future Work	38

A Related Works

Watermarking LLM-generated text. Watermarking in large language models (LLMs) can be broadly categorized into unbiased and biased approaches, both aiming to embed detectable signals without substantially degrading text quality. Unbiased watermarks preserve the original next-token distribution exactly. [1] draws independent pseudorandom variables and samples next token using a deterministic decoder, preserving the multinomial distribution via the Gumbel-max trick. Similarly, [18] generates the next token based on inverse transform sampling of the multinomial distribution. Optimal detection rules for these two unbiased LLM watermarks are derived under the statistical framework [19]. In contrast, biased watermarks perturb the token distribution to embed watermark signals. The KGW watermarking scheme [15] randomly partitions the token vocabulary into green and red lists and then increases the sampling probability of green tokens to create detectable deviations in green-token frequency. Subsequent works have focused on improving robustness [43] and optimizing the trade-off between detectability and text quality [33, 12]. Additionally, [35] and [34] proposed unbiased variants of the KGW watermark by introducing decoding algorithm based on maximal coupling and reweighting strategy, respectively. However, due to their reliance on the order of tokens, these text watermarking methods can not be directly applied to structural tabular data, where attacks like row reordering are so common.

Watermarking generated images. Image watermarking methods embed invisible signals either during training or sampling phase. [22] proposes a method to watermark pre-trained GANs without access to training data. [32] exploits DDIM invertibility to embed structural patterns into the frequency domain of the initial noise vector during sampling, achieving an effective and invisible image watermarking. [37] implements a performance-preserving watermarking for diffusion models by incorporating diffused bit information into Gaussian noise in the latent space. [46] has explored generalizing image watermarking techniques to structural tabular data. However, these methods still either fail to support row-wise detection or suffer from poor data fidelity and limited robustness.

Watermarking synthetic tabular data. Tabular watermarking methods primarily fall into two categories: sampling-phase watermarking and post-editing watermarking. The former embeds watermark into the latent space during the denoising generation phase or modifies the generative workflow. For instance, [46] implements row-wise watermark embedding using self-cloning and seeded shuffling techniques, ensuring close approximation to the standard Gaussian distribution. However, due to its reliance on large diffusion models using DDIM sampling strategy, this method is unsuitable for scenarios with limited GPU resources. [8] proposes MUSE, a model-agnostic method that selects watermarked rows via a pseudorandom scoring mechanism across multiple candidates, preserving fidelity but increasing generation cost. The latter offers lightweight watermarking by modifying synthesized tabular data after generation. [11] bins continuous feature values into predefined “green” intervals and [45] extends post-editing watermarking to tabular datasets with mixed-type features by selectively perturbing cells within a designated value range. While model-agnostic and computationally efficient, these approaches are either restricted by the feature type or vulnerable to noise and deletion attacks. The limitations of existing tabular watermarking methods highlight opportunities for improvement in four key dimensions: fidelity, detectability, applicability, and robustness. In this work, our proposed TAB-DRW addresses these limitations, achieving superior performance across all four dimensions.

B Privacy-Enhanced TAB-DRW

Inspired by the KGW watermark [15], we extend TAB-DRW with a privacy-enhanced variant designed to increase the difficulty of watermark removal. The modification is straightforward: prior to **Step 1** of watermark embedding, the columns of the tabular data are shuffled according to a pseudorandom permutation determined by the watermark key κ (which can be shared with the key in Algorithm 3), and after **Step 3**, the columns are reshuffled back to their original order. During detection, a verifier holding the correct key can reproduce the same column permutation to obtain the watermarked frequency-domain representation. See Figure 6 and Algorithm 2 for the complete procedure of the privacy-enhanced TAB-DRW.

Privacy-enhanced TAB-DRW satisfies two crucial requirements:

1. **The key-dependent variability in the frequency-domain representation does not substantially affect watermark distortion or detectability.** In other words, given randomly selected watermark keys, the privacy-enhanced TAB-DRW should exhibit nearly consistent performance in terms of data fidelity and watermark detectability. From a theoretical perspective, since P_κ is an orthogonal permutation matrix and the DFT/IDFT are unitary, inserting P_κ before and P_κ^{-1} after the frequency-domain transformation amounts to a norm-preserving change of entries in the original domain, meaning the total ℓ_2 distortion remains unchanged. Moreover, because detection evaluates sign alignment in the same keyed frequency coordinates, the resulting Z-score is invariant up to index relabeling. Empirical evidence supporting this claim is provided in Table 21 of Appendix G.4.

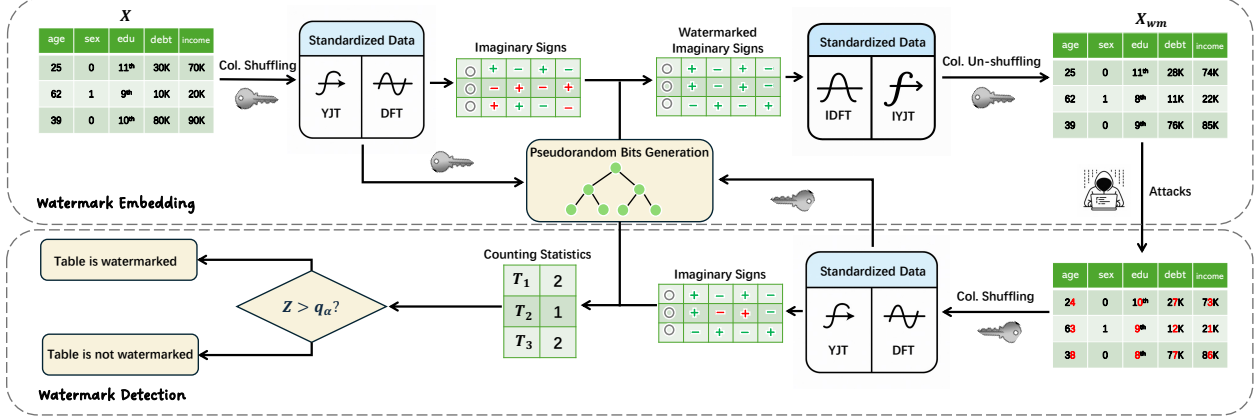


Figure 6: Work flow of privacy-enhanced TAB-DRW.

Algorithm 2 Watermarking embedding of privacy-enhanced TAB-DRW

- 1: **Input:** Tabular data $\mathbf{X} \in \mathbb{R}^{N \times p}$, parameters $\gamma \in [0, 1]$ and $\delta \in [-1, 1]$, watermark key κ .
 - 2: Shuffle \mathbf{X} using key-derived permutation P_κ to obtain $\mathbf{X}P_\kappa$.
 - 3: Transform $\mathbf{X}P_\kappa$ using YJT and standardization (still denoted as $\mathbf{X}P_\kappa$ for simplicity).
 - 4: **for** each row x in $\mathbf{X}P_\kappa$ **do**
 - 5: Compute $y \leftarrow \text{DFT}(x)$ and generate pseudorandom bits $\{\zeta_t\}_{t=1}^m$ via Algorithm 3.
 - 6: Modify y according to soft variant (2) to obtain y^{wm} .
 - 7: Recover $x^{\text{wm}} \leftarrow \text{IDFT}(y^{\text{wm}})$.
 - 8: **end for**
 - 9: Collect each x^{wm} to form a matrix \mathbf{X}^{wm} .
 - 10: Apply inverse standardization and inverse YJT to \mathbf{X}^{wm} , then unshuffle it to obtain $\mathbf{X}^{\text{wm}}P_\kappa^{-1}$.
 - 11: Perform rounding and clipping if needed, and release.
-

2. **The approach supports multi-key scenarios, as a watermark embedded with one key cannot be detected using another, thereby effectively avoiding false positives.** Furthermore, the collision-free key space must be sufficiently large to support large-scale deployment. The motivation behind this design lies in the sensitivity of the row-wise DFT to column order: frequency-domain representations derived from different pseudorandom permutations are nearly independent and exhibit nontrivial discrepancies. As a result, the watermark key is effectively encoded into the frequency-domain watermark signal as a unique, secret pattern. Furthermore, this sensitivity induces a combinatorially large key space of size $\mathcal{O}(p!)$ for a tabular dataset with p columns. Comprehensive empirical evaluations are presented in Table 22 of Appendix G.4.

C Missing Details from Section 2

Algorithm 3 details the steps to generate (during watermark embedding) or retrieve (during watermark detection) pseudorandom bit sequence for a target row $x^* \in \mathbb{R}^{1 \times p}$ within standardized tabular data $\mathbf{X} \in \mathbb{R}^{N \times p}$. We first sample a subset of column indices \mathcal{I} using the secret watermark key (Line 3). For each row, we compute the sum of entries in \mathcal{I} , based on which we obtain x_{rank}^* , the rank of the target row among all rows in \mathbf{X} . Then we normalize x_{rank}^* to $[0, 1]$ (Lines 4–6).

Next, We traverse an implicitly constructed binary tree of depth $\lceil \frac{m}{2} \rceil$, where each node deterministically binds with a bit pair, from the root down to a leaf. At each level j , we use x_{rank}^* to locate the underlying node and append its bit pair to the list \mathbf{S} (Lines 7–9, see Figure 7 for an illustration). Lines 8–9 define both the node-bit binding policy and the coupling rule between each of the $2^{\lceil \frac{m}{2} \rceil}$ equal-sized bins and the corresponding leaf nodes. Therefore, the above procedure is equivalent to traversing the path from the root to the leaf corresponding to the bin containing x_{rank}^* , as described in Section 2.3. Finally, we truncate \mathbf{S} to its first m entries to obtain the pseudorandom bit sequence for the target row. In practice, even if x_{rank}^* shifts to a neighboring leaf node due to post-processing attacks, the retrieved bit sequence differs from the original by only a bit pair, thanks to the tailored node-bits binding policy.

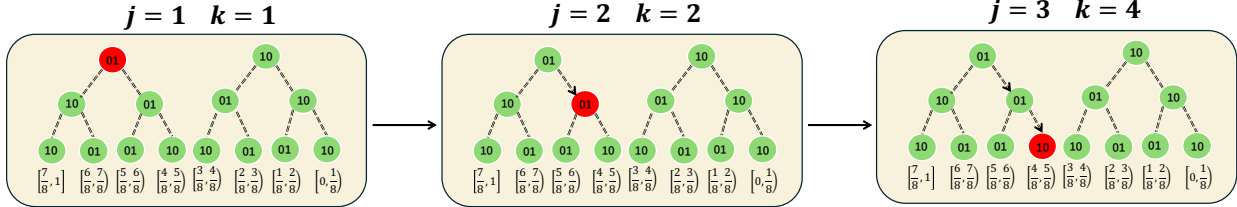


Figure 7: Illustration of Lines 7–9 in Algorithm 3 for the case $x_{\text{rank}}^* = 0.5$ and $m = 6$. The red circle highlights the k -th node at level j .

Algorithm 3 Row-wise Pseudorandom Bits Generation

- 1: **Input:** Standardized tabular data $\mathbf{X} \in \mathbb{R}^{N \times p}$, target row $\mathbf{x}^* \in \mathbb{R}^{1 \times p}$, and watermark key κ .
 - 2: **Initial:** An empty pseudorandom bit list \mathbf{S} , $m = \lfloor (p - 1)/2 \rfloor$.
 - 3: Sample a subset of column indices $\mathcal{I} \subset \{0, \dots, p - 1\}$ using κ .
 - 4: Compute the sum of selected entries for each row of \mathbf{X} .
 - 5: Compute the rank of the target row among all rows in \mathbf{X} to obtain x_{rank}^* .
 - 6: Normalize x_{rank}^* to lie in $[0, 1]$: $x_{\text{rank}}^* \leftarrow x_{\text{rank}}^*/(N - 1)$.
 - 7: **for** $j \leftarrow 1$ to $\lceil m/2 \rceil$ **do** ▷ Traverse the path from the root to the leaf.
 - 8: Locate the underlying node in the path: $k \leftarrow \lfloor 2^j \cdot x_{\text{rank}}^* \rfloor$.
 - 9: Append $[1, 0]$ to \mathbf{S} if $k \% 4 = 0$ or 3 ; else $[0, 1]$.
 - 10: **end for**
 - 11: Truncate \mathbf{S} to its first m entries, and release.
-

Connection to Gray codes. From the perspective of Gray codes, our pseudorandom bit generation scheme can be viewed as a special case of a 2-Gray code. We present the formal construction process below.

Let $n \in \mathbb{N}$. Denote by $\{0, 1\}^n$ the set of all binary strings of length n , and by $d_H(\cdot, \cdot)$ the Hamming distance on $\{0, 1\}^n$. Let $G_n = (g_0^n, g_1^n, \dots, g_{2^n-1}^n)$ with $g_i^n \in \{0, 1\}^n$ be a standard n -bit 1-Gray code, specified up to cyclic permutation. By definition, $d_H(g_i^n, g_{i+1}^n) = 1$ for all $i \in \{0, \dots, 2^n - 1\}$. We define the pair-encoding map $\varphi : \{0, 1\} \rightarrow \{0, 1\}^2$, $\varphi(0) = 10$, $\varphi(1) = 01$ and extend φ to a map $\phi : \{0, 1\}^n \rightarrow \{0, 1\}^{2n}$ by applying it coordinatewise: for $g^n = b_1 b_2 \dots b_n \in \{0, 1\}^n$, $b_j \in \{0, 1\}$, let $\phi(g^n) = \varphi(b_1) \varphi(b_2) \dots \varphi(b_n)$. For $n \in \mathbb{N}$, we then can define the set $H_{2n} = (h_0^{2n}, h_1^{2n}, \dots, h_{2^n-1}^{2n})$ and $H_{2n-1} = (\pi(h_0^{2n}), \pi(h_1^{2n}), \dots, \pi(h_{2^n-1}^{2n}))$, where $h_i^{2n} := \phi(g_i^n) \in \{0, 1\}^{2n}$ and $\pi : \{0, 1\}^{2n} \rightarrow \{0, 1\}^{2n-1}$ be the projection that deletes the last coordinate: $\pi(x_1, \dots, x_{2n}) = (x_1, \dots, x_{2n-1})$.

By construction, the family $\{H_n\}$ forms a collection of 2-Gray codes, and any two consecutive codewords h_i^n and h_{i+1}^n satisfy $d_H(h_i^n, h_{i+1}^n) \leq 2$. In our paper, a tree of depth N stores the sequence $\{H_n\}_{n=1}^{2N}$, and each rank bin corresponds to a distinct h_i^{2N} or $\pi(h_i^{2N})$. Compared with using a standard 1-Gray code, this construction has the advantage of slowing the growth rate of rank bins as the number of table columns increases, since $|H_n| = 2^{\lceil n/2 \rceil}$ whereas $|G_n| = 2^n$. This reduction leads to greater robustness of bit retrieval against rank shifts. In Appendix G.1, we provide additional evaluations on using a 1-Gray code for bit sequence generation .

D Missing Details from Section 3

Soundness of robustness analysis in the transformed domain. Our theoretical analysis is conducted entirely in the transformed domain, where both the original data \mathbf{X} and the watermarked data \mathbf{X}_{wm} have already been processed using the Yeo-Johnson transformation (YJT) and standardization. This setup deliberately omits the inverse YJT during watermark embedding and avoids re-estimating transformation parameters during watermark detection, thus ignoring the distribution shifts of watermarked frequency-domain representation caused by the parameters refitting.

Introducing an adaptive, nonlinear YJT transformation, where the parameter λ is estimated via maximum likelihood, would prevent us from obtaining a closed-form lower bound on the Z-score and would not offer additional insight into the core mechanism driving robustness. under the Gaussian assumption used in the analysis, the strong fidelity preservation of TAB-DRW keeps the watermarked data very close to the original Gaussian distribution. Consequently,

Table 6: YJT parameters summary (before vs. after watermarking) across varying dimensions and covariance structures.

Σ	N	p	λ Before	λ After	μ Before	μ After	σ Before	σ After
Identity	100	10	1.0164	1.0117	-0.0230	-0.0229	0.9792	0.9592
Identity	100	50	1.0065	1.0030	-0.0017	-0.0027	0.9957	0.9835
Identity	100	100	0.9743	0.9807	-0.0190	-0.0166	0.9917	0.9817
Identity	1000	10	1.0113	1.0113	0.0418	0.0420	1.0002	0.9883
Identity	1000	50	0.9971	0.9940	-0.0070	-0.0081	1.0020	0.9939
Identity	1000	100	0.9885	0.9861	-0.0056	-0.0064	1.0014	0.9943
Identity	10000	10	0.9970	0.9999	0.0017	0.0026	0.9988	0.9889
Identity	10000	50	1.0029	1.0027	0.0000	-0.0001	1.0000	0.9925
Identity	10000	100	1.0003	1.0011	0.0017	0.0020	0.9997	0.9930
AR(1)	100	10	0.9849	0.9735	0.0075	0.0028	1.0367	1.0231
AR(1)	100	50	1.0158	1.0128	0.0072	0.0064	0.9766	0.9680
AR(1)	100	100	0.9917	0.9921	-0.0222	-0.0223	0.9811	0.9724
AR(1)	1000	10	0.9866	0.9892	-0.0024	-0.0015	0.9963	0.9873
AR(1)	1000	50	0.9926	0.9911	-0.0046	-0.0051	0.9988	0.9926
AR(1)	1000	100	0.9972	0.9967	0.0010	0.0009	0.9954	0.9898
AR(1)	10000	10	1.0037	1.0051	0.0008	0.0013	0.9958	0.9873
AR(1)	10000	50	1.0023	1.0032	-0.0051	-0.0048	0.9998	0.9938
AR(1)	10000	100	0.9998	0.9998	-0.0001	-0.0000	0.9999	0.9946

Table 7: Detection performance under different parameter-refitting settings. Each entry reports the average Z-score over 1K rows, evaluated using TAB-DRW with $(\gamma, \delta) = (0.5, 0.5)$ under 100 trials.

Dataset	Idealized setting	Practical setting
Adult	15.13 ± 1.04	12.81 ± 1.17
Magic	30.47 ± 0.85	27.34 ± 0.93
Shoppers	21.14 ± 0.84	18.18 ± 1.28
Default	19.02 ± 0.85	15.98 ± 0.92
Drybean	41.36 ± 0.98	38.03 ± 1.03

the effect of YJT refitting on both the data distribution and the watermark signal induced by sign-bit alignment is minimal. This makes the idealized model appropriate for the theoretical robustness study, and it does not alter the conclusions we derive.

To validate our point above, we provide a case study to illustrate the minimal difference between the original YJT parameters and those refitted after watermark embedding. Specifically, we generate multivariate Gaussian tables with row counts $N \in \{100, 1000, 10000\}$ and column counts $p \in \{10, 50, 100\}$. Two covariance structures are considered: the identity matrix and an AR(1) matrix $\Sigma_{ij} = \rho^{|i-j|}$ with $\rho = 0.4$. Each table is watermarked using TAB-DRW with $(\gamma, \delta) = (0.5, 0.5)$. The YJT parameters λ , mean μ , and standard deviation σ are recorded before and after watermarking and averaged across all columns. The results in Table 6 show that TAB-DRW introduces negligible perturbations to these parameters across different dimensions and covariance structures.

We also provide additional empirical evaluations by comparing detection performance under 1) **idealized setting**: No parameter refitting, as assumed in Section 3, and 2) **practical setting**: With parameter refitting, as used in experiments. As shown in Table 7, the impact of distribution shifts on detection performance is negligible relative to post-processing attacks, and the embedded watermark remains highly detectable even under such shifts. These results demonstrate both the robustness of our approach and the validity of conducting robustness analysis in the transformed domain.

Soundness of robustness analysis under Gaussian assumption. Real-world tabular data are highly heterogeneous and rarely follow a strict multivariate Gaussian distribution. However, after applying the Yeo–Johnson transformation (YJT), the data typically become much closer to Gaussian. As discussed earlier, YJT standardizes heterogeneous feature scales and reduces skewness, enabling more tractable analysis in the transformed space.

Although the Gaussian assumption does not fully capture the complexity of real-world data, deriving closed-form robustness guarantees under arbitrary, non-Gaussian distributions is generally intractable. Our aim is not to provide universal theoretical guarantees, but to clarify the underlying robustness mechanism of our method. In particular, we

show how sign alignment in the frequency domain, together with the hyperparameters (γ, δ) , preserves the watermark signal under perturbations. Therefore, we adopt the multivariate Gaussian model as a simplified yet widely used analytical tool to make this intuition concrete. As the saying goes, “All models are wrong, but some are useful.” Our analysis is intended to shed light on why our method is robust—not to claim robustness under all possible data distributions.

To extend our robustness analysis to a broader class of distributions, we relax the Gaussian assumption to a sub-Gaussian setting and derive a corresponding lower bound on the Z-score under noise corruption. This setting accommodates features with light-tailed distributions, including bounded or discrete categorical features. See formal theorems and proof details in Appendix E.4.

E Theoretical Analysis and Proofs

E.1 Proof of Proposition 1

Proof of Proposition 1. Let $\Delta y_{i,j} = y_{i,j}^{\text{wm}} - y_{i,j}$ denote the entry-wise difference in the frequency domain, then by Def. 2 and the Algorithm 1 with soft parameters (γ, δ) , we have

$$\Delta y_{i,k} = \begin{cases} -i(1+\delta) \cdot \Im(y_{i,k}), & k \in S, \\ i(1+\delta) \cdot \Im(y_{i,p-k}), & p-k \in S, \\ 0, & \text{otherwise.} \end{cases}$$

By the inverse DFT as defined in Def. 2, the entry-wise difference $\Delta x_{i,j}$ is given by

$$\begin{aligned} \Delta x_{i,j} &= \frac{1}{\sqrt{p}} \left[\sum_{k \in S} \Delta y_{i,k} e^{i \frac{2\pi}{p} kj} + \sum_{p-k \in S} \Delta y_{i,k} e^{i \frac{2\pi}{p} kj} \right] \\ &= \frac{2(1+\delta)}{\sqrt{p}} \left[\sum_{k \in S} \Im(y_{i,k}) \sin \frac{2\pi}{p} kj \right]. \end{aligned}$$

Plugging in $\Im(y_{i,k}) = -\frac{1}{\sqrt{p}} \sum_{n=0}^{p-1} x_{in} \sin \frac{2\pi kn}{p}$ leads to

$$\Delta x_{i,j} = -\frac{2(1+\delta)}{p} \sum_{n=0}^{p-1} \left[\sum_{k \in S} \sin \frac{2\pi kn}{p} \sin \frac{2\pi kj}{p} \right] x_{in},$$

which is precisely $\Delta x_{i,j} = -\alpha \beta_j^\top \mathbf{x}_i$ with $\alpha = \frac{2(1+\delta)}{p}$ and the stated β_j and \mathbf{x}_i . \square

E.2 Proof of Theorem 1

We prove items one by one.

1. **Mean.** For each column $j = 0, \dots, p-1$, we have

$$\frac{1}{N} \sum_{i=1}^N \Delta x_{i,j} = -\alpha \beta_j^\top \left(\frac{1}{N} \sum_{i=1}^N \mathbf{x}_i \right) = 0,$$

since each column is centered.

2. **Pearson correlation coefficients (PCC).** Given that each column is centered and standardized, the difference of PCC between each column pair (j, ℓ) is given by

$$\Delta r_{j\ell} = \frac{1}{N} \sum_{i=1}^N (x_{i,j} \Delta x_{i,\ell} + x_{i,\ell} \Delta x_{i,j} + \Delta x_{i,j} \Delta x_{i,\ell}).$$

Plugging $\Delta x_{i,j} = -\alpha \beta_j^\top \mathbf{x}_i$ leads to

$$\Delta r_{j\ell} = -\alpha ([\Sigma \beta_\ell]_j + [\Sigma \beta_j]_\ell) + \alpha^2 \beta_j^\top \Sigma \beta_\ell,$$

where $\Sigma = \frac{1}{N} \mathbf{X}^\top \mathbf{X}$ with $\text{diag}(\Sigma) = \mathbb{I}$.

3. **Empirical distribution.** Consider the coupling matching $x_{i,j}$ to $x_{i,j} + \Delta x_{i,j}$ for each i , we bound the transport cost as below:

$$\mathcal{W}_2^2(\rho_j, \nu_j) \leq \frac{1}{N} \sum_{i=1}^N (\Delta x_{i,j})^2 = \alpha^2 \boldsymbol{\beta}_j^\top \boldsymbol{\Sigma} \boldsymbol{\beta}_j,$$

which leads to the claimed inequality.

E.3 Proof of Theorem 2

Lemma 1 (Gaussian tail bound). *Let $\Phi(u)$ denote the standard normal CDF and $Q(u) := 1 - \Phi(u)$. For any $u > 0$,*

$$Q(u) \leq \frac{1}{2} e^{-u^2/2}.$$

Proof of Lemma 1. We discuss the bound under two cases.

Case 1: When $u > \sqrt{\frac{2}{\pi}}$, through integration by parts, we have

$$Q(u) = \frac{1}{\sqrt{2\pi}} \int_u^\infty e^{-t^2/2} dt \leq \frac{1}{\sqrt{2\pi}} \left[\frac{e^{-u^2/2}}{u} - \int_u^\infty \frac{e^{-t^2/2}}{t^2} dt \right].$$

Dropping the negative integral preserves the inequality, yielding

$$Q(u) \leq \frac{1}{u\sqrt{2\pi}} e^{-u^2/2} \leq \frac{1}{2} e^{u^2/2}.$$

Case 2: When $0 < u \leq \sqrt{\frac{2}{\pi}}$, we have

$$\frac{d}{du} \left(\frac{1}{2} e^{-u^2/2} \right) = -\frac{u}{2} e^{-u^2/2} \geq -\frac{1}{\sqrt{2\pi}} e^{-u^2/2} = \frac{d}{du} Q(u),$$

where the inequality follows from $u \leq \sqrt{\frac{2}{\pi}}$. Integrating from 0 to u gives

$$\int_0^u d \left(\frac{1}{2} e^{-t^2/2} \right) \geq \int_0^u dQ(t) \Rightarrow Q(u) \leq \frac{1}{2} e^{-u^2/2}.$$

Combining the two cases yields the stated bound. \square

Lemma 2 (Noise in the frequency domain). *Let $\boldsymbol{\varepsilon} = (\varepsilon_0, \dots, \varepsilon_{p-1})^\top \sim \mathcal{N}(\mathbf{0}, \sigma^2 \mathbf{I}_p)$ be a real-valued Gaussian noise vector of length p . Apply the DFT in Def. 2 to obtain $\hat{\boldsymbol{\varepsilon}} = (\hat{\varepsilon}_0, \dots, \hat{\varepsilon}_{p-1})^\top$. Denote by*

$$z_t = \Im(\hat{\varepsilon}_t), \quad t = 1, \dots, m,$$

the imaginary part of the noise component at the t -th effective entry. Then

$$z_t \sim \mathcal{N}\left(0, \frac{\sigma^2}{2}\right).$$

Proof of Lemma 2. Denote $\theta_{t,n} := \frac{2\pi tn}{p}$, we have

$$z_t = -\frac{1}{\sqrt{p}} \sum_{n=0}^{p-1} \varepsilon_n \sin(\theta_{t,n}).$$

Note that z_t is a linear combination of independent Gaussian variables, hence still be a Gaussian with zero mean. Since $\text{Var}(\varepsilon_n) = \sigma^2$ and the ε_n 's are independent,

$$\text{Var}[z_t] = \frac{1}{p} \sigma^2 \sum_{n=0}^{p-1} \sin^2(\theta_{t,n}).$$

Using the trigonometric identity $\sin^2 u = \frac{1}{2}(1 - \cos 2u)$,

$$\sum_{n=0}^{p-1} \sin^2(\theta_{t,n}) = \frac{p}{2} - \frac{1}{2} \sum_{n=0}^{p-1} \cos(2\theta_{t,n}).$$

The second sum is a geometric series whose value is 0 whenever $t \notin \{0, \frac{p}{2}\}$:

$$\sum_{n=0}^{p-1} e^{i \frac{4\pi tn}{p}} = \frac{1 - e^{i 4\pi t}}{1 - e^{i \frac{4\pi t}{p}}} = 0.$$

Hence $\sum_{n=0}^{p-1} \sin^2(\theta_{t,n}) = \frac{p}{2}$ for each $t = 1, \dots, m$. Substituting back,

$$\text{Var}[z_t] = \frac{\sigma^2}{p} \cdot \frac{p}{2} = \frac{\sigma^2}{2}.$$

□

Lemma 3 (Standard Z-score). *If pseudorandom bits $\zeta_{i,j} \stackrel{\text{i.i.d.}}{\sim} \text{Bernoulli}(0.5)$ and are independent of effective entries $\{y_{i,j}\}$, then $\{T_i\}_{i=1}^N$, as defined in Section 2, i.i.d. follows $B(m, \frac{1}{2})$ under H_0 , thus has expected value $\frac{m}{2}$ and variance $\frac{m}{4}$. By Central Limit Theorem, the Z-score under H_0 follows*

$$Z = \frac{\sum_{i=1}^N T_i - \frac{mN}{2}}{\sqrt{\frac{mN}{4}}} \xrightarrow{d} \mathcal{N}(0, 1) \text{ as } N \rightarrow \infty.$$

Proof of Lemma 3. For each index pair (i, j) of effective entries, define the events

$$E_{i,j} := \{\text{sign}(\Im(y_{i,j})) = 2\zeta_{i,j} - 1\}, \quad A_{i,j} := \{\text{sign}(\Im(y_{i,j})) = 1\}.$$

We will show that the indicator variables $\{\mathbb{I}(E_{i,j})\}_{i,j}$ are independent and identically distributed as Bernoulli(0.5).

First, set

$$p_{i,j} := \mathbb{P}(\text{sign}(\Im(y_{i,j})) = 1).$$

By conditioning on $\zeta_{i,j} \in \{0, 1\}$ and using the fact that $\mathbb{P}(\zeta_{i,j} = 1) = \mathbb{P}(\zeta_{i,j} = 0) = \frac{1}{2}$, we obtain

$$\mathbb{P}(E_{i,j}) = p_{i,j} \mathbb{P}(\zeta_{i,j} = 1) + (1 - p_{i,j}) \mathbb{P}(\zeta_{i,j} = 0) = \frac{1}{2} p_{i,j} + \frac{1}{2} (1 - p_{i,j}) = \frac{1}{2}.$$

Hence each $\mathbb{I}(E_{i,j}) \sim \text{Bernoulli}(0.5)$.

To verify independence, for any finite index set $\mathcal{I} \subseteq \{(i, j) : 1 \leq i \leq N, 1 \leq j \leq m\}$. we consider a family of events

$$\mathcal{B} = \{B_{\mathcal{I}_1, \mathcal{I}_2} : \mathcal{I}_1 \cup \mathcal{I}_2 = \mathcal{I}, \mathcal{I}_1 \cap \mathcal{I}_2 = \emptyset\}, \quad B_{\mathcal{I}_1, \mathcal{I}_2} = \left(\bigcap_{(i,j) \in \mathcal{I}_1} A_{i,j} \right) \cap \left(\bigcap_{(i,j) \in \mathcal{I}_2} A_{i,j}^c \right).$$

Clearly \mathcal{B} is a partition of the sample space Ω , hence we have

$$\begin{aligned} \mathbb{P}\left(\bigcap_{(i,j) \in \mathcal{I}} E_{i,j}\right) &= \sum_{B_{\mathcal{I}_1, \mathcal{I}_2} \in \mathcal{B}} \mathbb{P}(B_{\mathcal{I}_1, \mathcal{I}_2}) \prod_{(i,j) \in \mathcal{I}_1} \mathbb{P}(\zeta_{i,j} = 1) \prod_{(i,j) \in \mathcal{I}_2} \mathbb{P}(\zeta_{i,j} = 0) \\ &= \sum_{B_{\mathcal{I}_1, \mathcal{I}_2} \in \mathcal{B}} \mathbb{P}(B_{\mathcal{I}_1, \mathcal{I}_2}) \frac{1}{2^{|\mathcal{I}|}} = \frac{1}{2^{|\mathcal{I}|}} = \prod_{(i,j) \in \mathcal{I}} \mathbb{P}(E_{i,j}), \end{aligned}$$

This implies that the collection of events $\{E_{i,j}\}_{i,j}$ is mutually independent. Together with the fact that $\mathbb{P}(E_{i,j}) = \frac{1}{2}$, this completes the proof.

□

Proof of Theorem 2. We continue with the notations established in Lemmas 2 and 3. Let

$$\mathbf{X} = \{x_{i,j}\} \in \mathbb{R}^{N \times p}, \quad \mathbf{x}_i := (x_{i,0}, \dots, x_{i,p-1}) \stackrel{\text{i.i.d.}}{\sim} \mathcal{N}(0, \Sigma),$$

and denote the frequency-domain representation by $\mathbf{Y} \in \mathbb{C}^{N \times p}$. Then for each row, the effective entries satisfy:

$$\Im(y_t) = -\frac{1}{\sqrt{p}} \sum_{n=0}^{p-1} x_n \sin(\theta_{t,n}),$$

where $\theta_{t,n} = \frac{2\pi tn}{p}$. Let \mathbf{s}_t denotes $(\sin(\theta_{t,0}), \dots, \sin(\theta_{t,p-1})) \in \mathbb{R}^{1 \times p}$. Since each x_i is Gaussian, $\Im(y_t)$ is Gaussian with zero mean and

$$\text{Var}[\Im(y_t)] = \frac{1}{p} \mathbf{s}_t^\top \Sigma \mathbf{s} \in \left[\frac{\lambda_{\min}}{p} \|\mathbf{s}_t\|_2^2, \frac{\lambda_{\max}}{p} \|\mathbf{s}_t\|_2^2 \right] = \left[\frac{\lambda_{\min}}{2}, \frac{\lambda_{\max}}{2} \right],$$

where $\|\mathbf{s}_t\|_2^2 = \frac{p}{2}$ follows from Lemma 2 and λ_{\min} and λ_{\max} denote the smallest and largest eigenvalue of the covariance matrix Σ , respectively.

Given a pseudorandom bit $\zeta_t \in \{0, 1\}$, the process of watermark embedding in Algorithm 1 replaces $\Im(y_t)$ by

$$\Im(y_t^{\text{wm}}) = \begin{cases} -\delta \cdot \Im(y_t), & \text{if } \Im(y_t) \cdot (2\zeta_t - 1) < 0 \text{ and } |\Im(y_t)| \leq \text{Quantile}_\gamma(\{|\Im(y_t)|\}_{t=1}^m), \\ \Im(y_t), & \text{otherwise,} \end{cases}$$

Let

$$\alpha_t := |\Im(y_t^{\text{wm}})|, \quad \frac{\lambda}{2} := \text{Var}[\Im(y_t)] \in \left[\frac{\lambda_{\min}}{2}, \frac{\lambda_{\max}}{2} \right],$$

and define

$$F(x) := \frac{2}{\sqrt{\pi\lambda}} e^{-\frac{x^2}{\lambda}} \mathbb{I}(x \geq 0), \quad F_\delta(x) := \frac{2}{\delta\sqrt{\pi\lambda}} \exp\left(-\frac{x^2}{\delta^2\lambda}\right) \mathbb{I}(x \geq 0),$$

which are the PDFs of α_t and $\delta \alpha_t$, respectively. Under large p , there are three scenarios for each t :

- **Case 1:** With probability $\frac{1}{2}$, $\alpha_t \sim F$ and $\Im(y_t^{\text{wm}}) \cdot (2\zeta_t - 1) > 0$.
- **Case 2:** With probability $\frac{\gamma}{2}$, $\alpha_t \sim F_\delta$ and $\Im(y_t^{\text{wm}}) \cdot (2\zeta_t - 1) > 0$.
- **Case 3:** With probability $\frac{1-\gamma}{2}$, $\alpha_t \sim F$ and $\Im(y_t^{\text{wm}}) \cdot (2\zeta_t - 1) < 0$.

Sign-flip probability under additive noise. Let $z_t \sim \mathcal{N}(0, \frac{\sigma^2}{2})$ be the imaginary-part noise as derived in Lemma 2. Conditioned on $\alpha_t = x$, the probability that noise flips the sign of $\Im(y_t^{\text{wm}})$ in **Case 1** and **Case 3** is

$$\begin{aligned} \mathbb{P}_{\text{flip}}(\sigma) &= \mathbb{P}(z_t > \alpha_t | \alpha_t \sim F) \\ &= \int_0^\infty \mathbb{P}(z_t > \alpha_t | \alpha_t = x) F(x) dx \\ &= \int_0^\infty \frac{2}{\sqrt{\pi\lambda}} e^{-\frac{x^2}{\lambda}} Q\left(\frac{\sqrt{2}x}{\sigma}\right) dx \\ &\leq \frac{1}{\sqrt{\pi\lambda_{\min}}} \int_0^{\sqrt{\frac{\lambda_{\min}}{2}}} e^{-x^2\left(\frac{1}{\lambda_{\min}} + \frac{1}{\sigma^2}\right)} dx \\ &\quad + \frac{1}{\sqrt{\pi\lambda_{\max}}} \int_{\sqrt{\frac{\lambda_{\max}}{2}}}^\infty e^{-x^2\left(\frac{1}{\lambda_{\max}} + \frac{1}{\sigma^2}\right)} dx \\ &\quad + \frac{e^{-\frac{1}{2}}}{\sqrt{2\pi}} \int_{\sqrt{\frac{\lambda_{\min}}{2}}}^{\sqrt{\frac{\lambda_{\max}}{2}}} \frac{e^{-\frac{x^2}{\sigma^2}}}{x} dx \\ &= \frac{\sigma}{\sqrt{\sigma^2 + \lambda_{\min}}} \left[\Phi\left(\sqrt{1 + \frac{\lambda_{\min}}{\sigma^2}}\right) - \frac{1}{2} \right] \\ &\quad + \frac{\sigma}{\sqrt{\sigma^2 + \lambda_{\max}}} \left[1 - \Phi\left(\sqrt{1 + \frac{\lambda_{\max}}{\sigma^2}}\right) \right] \end{aligned}$$

$$+ \frac{1}{\sqrt{8\pi e}} \left[E_1\left(\frac{\lambda_{\min}}{2\sigma^2}\right) - E_1\left(\frac{\lambda_{\max}}{2\sigma^2}\right) \right],$$

where the inequality follows from Lemma 1 and the local monotonicity of $F(x)$. Similarly, if the amplitude of α_t is scaled by δ , we obtain $\mathbb{P}_{\text{flip}}^{(\delta)}(\sigma) = \mathbb{P}(z_t > \alpha_t | \alpha_t \sim F_\delta) \leq \mathcal{I}(\frac{\sigma}{\delta})$, where

$$\mathcal{I}(s) := \frac{s}{\sqrt{s^2 + \lambda_{\min}}} \left[\Phi\left(\sqrt{1 + \frac{\lambda_{\min}}{s^2}}\right) - \frac{1}{2} \right] + \frac{s}{\sqrt{s^2 + \lambda_{\max}}} \left[1 - \Phi\left(\sqrt{1 + \frac{\lambda_{\max}}{s^2}}\right) \right] + \frac{1}{\sqrt{8\pi e}} \left[E_1\left(\frac{\lambda_{\min}}{2s^2}\right) - E_1\left(\frac{\lambda_{\max}}{2s^2}\right) \right].$$

Alignment probability after attack. Let $p_{i,j}$ be the probability that the j -th effective entry in row i maintains alignment with its corresponding pseudorandom bit under attack. Combining the three cases above, we have

$$\begin{aligned} p_{i,j} &= \frac{1}{2} (1 - \mathbb{P}_{\text{flip}}(\sigma)) + \frac{\gamma}{2} \left(1 - \mathbb{P}_{\text{flip}}^{(\delta)}(\sigma) \right) + \frac{1-\gamma}{2} \mathbb{P}_{\text{flip}}(\sigma) \\ &= \frac{1+\gamma}{2} - \frac{\gamma}{2} \left[\mathbb{P}_{\text{flip}}(\sigma) + \mathbb{P}_{\text{flip}}^{(\delta)}(\sigma) \right] \\ &\geq \frac{1+\gamma}{2} - \frac{\gamma}{2} \left[\mathcal{I}(\sigma) + \mathcal{I}\left(\frac{\sigma}{\delta}\right) \right] \end{aligned} \tag{5}$$

Lower bound on the expected Z-score. Under this setting, we recall Lemma 3 for the standard Z-score $Z = \frac{\sum_{i,j} \mathbb{I}\{E_{i,j}\} - \frac{mN}{2}}{\sqrt{\frac{mN}{4}}}$, then we obtain

$$\mathbb{E}[Z(\gamma, \delta, \sigma)] = \frac{mN p_{i,j} - \frac{mN}{2}}{\sqrt{\frac{mN}{4}}} \geq \sqrt{mN} \gamma \left[1 - \mathcal{I}(\sigma) - \mathcal{I}\left(\frac{\sigma}{\delta}\right) \right],$$

which completes the proof. \square

E.4 Further Analysis on Robustness

Based on the assumption and notations in Theorem 2, we also derived a conservative, non-asymptotic lower bound on the number of rows N required to achieve a statistical test with power $1 - \beta$ at significance level α . Theorem 3 gives a formal description. Since real-world tabular data are highly heterogeneous and rarely follow a strict multivariate Gaussian distribution even after YJT, we relax the Gaussian assumption in Theorem 2 to a sub-Gaussian setting and provide a corresponding lower bound on the Z-score under noise corruption. This setting accommodates features with light-tailed distributions, including bounded or discrete categorical features. A formal statement is given in Theorem 4.

Theorem 3. We assume that unwatermarked tabular data \mathbf{X} has rows $\mathbf{x}_i \stackrel{\text{i.i.d.}}{\sim} \mathcal{N}(0, \Sigma)$, where $\Sigma \in \mathbb{R}^{p \times p}$ is positive-definite. Denote the smallest and largest eigenvalue of Σ by λ_{\min} and λ_{\max} , respectively. Define $N_{\alpha, \beta}(\gamma, \delta, \sigma)$ as the number of rows required for the Gaussian noise-corrupted table $\mathbf{X}_{\text{wm}} + \varepsilon$ to achieve a statistical test with power $1 - \beta$ at significance level α , where \mathbf{X}_{wm} denote the table watermarked under soft hyperparameters (γ, δ) and $\varepsilon_{i,j} \stackrel{\text{i.i.d.}}{\sim} \mathcal{N}(0, \sigma^2)$. Then, for any $\gamma, \alpha, \beta \in [0, 1]$ and $\delta, \sigma > 0$,

$$N_{\alpha, \beta}(\gamma, \delta, \sigma) \geq \frac{\left[q_\alpha + \sqrt{2m \ln\left(\frac{1}{\beta}\right)} \right]^2}{m\gamma^2 \left[1 - \mathcal{I}(\sigma) - \mathcal{I}\left(\frac{\sigma}{\delta}\right) \right]^2}, \tag{6}$$

where $m = \lfloor \frac{p-1}{2} \rfloor$ and q_α is the critical value for a one-sided test at level α . The function $\mathcal{I} : (0, \infty) \rightarrow \mathbb{R}$ is defined as

$$\mathcal{I}(s) := \frac{s}{\sqrt{s^2 + \lambda_{\min}}} \left[\Phi\left(\sqrt{1 + \frac{\lambda_{\min}}{s^2}}\right) - \frac{1}{2} \right] + \frac{s}{\sqrt{s^2 + \lambda_{\max}}} \left[1 - \Phi\left(\sqrt{1 + \frac{\lambda_{\max}}{s^2}}\right) \right] + \frac{1}{\sqrt{8\pi e}} \left[E_1\left(\frac{\lambda_{\min}}{2s^2}\right) - E_1\left(\frac{\lambda_{\max}}{2s^2}\right) \right].$$

with $\Phi(\cdot)$ denoting the standard normal CDF and $E_1(u) = \int_u^\infty \frac{e^{-t}}{t} dt$ the exponential integral.

Proof of Theorem 3. Denote the random variables after noise perturbation as below: $I_{i,j} := \mathbb{I}\{\Im(y_{i,j})(2\zeta_{i,j} - 1) > 0\}$, $T_i := \sum_{j=1}^m I_{i,j}$, and $S_N := \sum_{i=1}^N T_i$. We omit their explicit dependence on hyperparameters (γ, δ, σ) here for simplicity. From Lemma 3, the Z-score follows

$$Z = \frac{S_N - \frac{mN}{2}}{\sqrt{\frac{mN}{4}}}.$$

By Eq.(5), we have

$$\mathbb{E}_{H_1}[S_N] = \sum_{i=1}^N \sum_{j=1}^m p_{i,j} \geq mN \left(\frac{1+\gamma}{2} - \frac{\gamma}{2} \left[\mathcal{I}(\sigma) + \mathcal{I}\left(\frac{\sigma}{\delta}\right) \right] \right).$$

Then for a one-sided level- α test with threshold q_α , we have

$$\{Z \leq q_\alpha\} \subseteq \{S_N - \mathbb{E}_{H_1}[S_N] \leq -t_N\}, \quad t_N := \left(\sqrt{mN} \gamma \left[1 - \mathcal{I}(\sigma) - \mathcal{I}\left(\frac{\sigma}{\delta}\right) \right] - q_\alpha \right) \frac{\sqrt{mN}}{2},$$

Since T_i are independent and bounded in $[0, m]$ (i.i.d. rows and row-wise watermarking), We apply Hoeffding's inequality:

$$\mathbb{P}_{H_1}\{Z \leq q_\alpha\} \leq \exp\left(-\frac{2t_N^2}{Nm^2}\right) = \exp\left(-\frac{\left(\sqrt{mN}\gamma\left[1 - \mathcal{I}(\sigma) - \mathcal{I}\left(\frac{\sigma}{\delta}\right)\right] - q_\alpha\right)^2}{2m}\right).$$

Imposing $\mathbb{P}_{H_1}\{Z \leq q_\alpha\} \leq \beta$ gives a conservative lower bound:

$$\sqrt{mN}\gamma\left[1 - \mathcal{I}(\sigma) - \mathcal{I}\left(\frac{\sigma}{\delta}\right)\right] \geq q_\alpha + \sqrt{2m\ln(1/\beta)},$$

which implies the nonasymptotic sample-size lower bound to achieve a test of power $1 - \beta$ at level α :

$$N_{\alpha,\beta}(\gamma, \delta, \sigma) \geq \frac{\left[q_\alpha + \sqrt{2m\ln\left(\frac{1}{\beta}\right)}\right]^2}{m\gamma^2 \left[1 - \mathcal{I}(\sigma) - \mathcal{I}\left(\frac{\sigma}{\delta}\right)\right]^2}.$$

□

The Remark 4 below provides a numerical illustration of Theorem 3.

Remark 4. We provide a numerical example to illustrate the guarantee in Theorem 3. When $p = 11$ ($m = 5$) and $\Sigma = \mathbb{I}_{p \times p}$, the theoretical lower bound (the right-hand side of (6)) for the number of rows N required to achieve a test of power $1 - \beta = 0.99$ at level $\alpha = 0.001$, i.e. 0.99 TPR@0.1%FPR, is given by:

$$N_{0.001,0.01}(0.5, 0.5, \sigma) \geq \begin{cases} 108, & \text{if } \sigma = 0.1, \\ 153, & \text{if } \sigma = 0.2, \\ 437, & \text{if } \sigma = 0.5. \end{cases}$$

Theorem 4 (Robustness under sub-Gaussian samples). *Assume that unwatermarked tabular data $\mathbf{X} \in \mathbb{R}^{N \times p}$ has i.i.d. rows $\mathbf{x}_i \in \mathbb{R}^p$ with zero mean and covariance $\Sigma \in \mathbb{R}^{p \times p}$, and are Σ -sub-Gaussian, meaning there exists $\kappa \geq 1$ such that for every $u \in \mathbb{R}^p$, $\|\langle u, \mathbf{x}_i \rangle\|_{\psi_2} \leq \kappa \sqrt{u^\top \Sigma u}$ [29]. Denote the smallest eigenvalue of Σ by λ_{\min} . Define $Z(\gamma, \delta, \sigma)$ as the standard Z-score (as in (3)) computed on the Gaussian noise-corrupted table $\mathbf{X}_{wm} + \varepsilon$, where $\mathbf{X}_{wm} \in \mathbb{R}^{N \times p}$ denote the table watermarked under soft hyperparameters (γ, δ) and $\varepsilon_{i,j} \stackrel{\text{i.i.d.}}{\sim} \mathcal{N}(0, \sigma^2)$. Fix any $\theta \in (0, 1)$ and let $C_4 > 0$ denote a constant such that for every real sub-Gaussian U with variance v we have $\mathbb{E}U^4 \leq C_4 \kappa^4 v^2$. Define $\rho(\kappa, \theta) := \frac{(1-\theta)^2}{2C_4 \kappa^4}$. Then, for any $\gamma \in [0, 1]$ and $\delta, \sigma > 0$,*

$$\mathbb{E}[Z(\gamma, \delta, \sigma)] \geq \sqrt{mN} \gamma \sup_{\theta \in (0, 1)} \left\{ \rho(\kappa, \theta) \left[2 - \exp\left(-\frac{\theta \lambda_{\min}}{2\sigma^2}\right) - \exp\left(-\frac{\theta \lambda_{\min} \delta^2}{2\sigma^2}\right) \right] \right\}.$$

Proof of Theorem 4. Let $\mathbf{x} = (x_0, \dots, x_{p-1})$ be a standardized row and $\mathbf{y} = \text{DFT}(\mathbf{x})$. For the t -th effective frequency, we have

$$\Im(y_t) = -\frac{1}{\sqrt{p}} \sum_{n=0}^{p-1} x_n \sin\left(\frac{2\pi tn}{p}\right) = -\frac{1}{\sqrt{p}} \mathbf{s}_t^\top \mathbf{x}, \quad \|\mathbf{s}_t\|_2^2 = \sum_{n=0}^{p-1} \sin^2\left(\frac{2\pi tn}{p}\right) = \frac{p}{2}.$$

By the Σ -sub-Gaussian assumption and linearity, $\Im(y_t)$ is sub-Gaussian with

$$v_t := \text{Var}[\Im(y_t)] = \frac{1}{p} \mathbf{s}_t^\top \Sigma \mathbf{s}_t \in \left[\frac{\lambda_{\min}}{2}, \frac{\lambda_{\max}}{2} \right], \quad \|\Im(y_t)\|_{\psi_2} = \left\| -\frac{1}{\sqrt{p}} \mathbf{s}_t^\top \mathbf{x} \right\|_{\psi_2} \leq \kappa \sqrt{v_t}.$$

Let $\alpha_t := |\Im(y_t^{\text{wm}})|$ and $z_t := \Im(\hat{\varepsilon}_t) \sim N(0, \sigma^2/2)$ be the imaginary-part noise (Lemma 2). Following the analysis in Theorem 2, for each effective entry the alignment probability with its bit satisfies

$$p_{i,j} = \frac{1+\gamma}{2} - \frac{\gamma}{2} \left(\mathbb{P}_{\text{flip}}(\sigma) + \mathbb{P}_{\text{flip}}^{(\delta)}(\sigma) \right), \quad (7)$$

where $\mathbb{P}_{\text{flip}}(\sigma) = \mathbb{E}[\mathbb{I}\{z_t > \alpha_t\}] = \mathbb{E}[Q(\sqrt{2}\alpha_t/\sigma)]$, and $\mathbb{P}_{\text{flip}}^{(\delta)}$ is the same quantity with the amplitude scaled by $|\delta|$. Here $Q(u) = 1 - \Phi(u)$.

By Lemma 1, $Q(u) \leq \frac{1}{2}e^{-u^2/2}$, hence $\mathbb{P}_{\text{flip}}(\sigma) \leq \frac{1}{2}\mathbb{E}\exp(-\alpha_t^2/\sigma^2)$. Write $U := \Im(y_t)$ and $Y := U^2$. For any $\theta \in (0, 1)$, Paley-Zygmund inequality gives

$$\mathbb{P}(Y \geq \theta \mathbb{E}Y) \geq \frac{(1-\theta)^2 (\mathbb{E}Y)^2}{\mathbb{E}Y^2} = \frac{(1-\theta)^2 v_t^2}{\mathbb{E}U^4} \geq \frac{(1-\theta)^2}{C_4 \kappa^4} =: \eta,$$

where we used the sub-Gaussian fourth-moment bound $\mathbb{E}U^4 \leq C_4 \kappa^4 v_t^2$. Thus, by conditioning on the event $\{Y \geq \theta v_t\}$,

$$\mathbb{E}\exp(-\alpha_t^2/\sigma^2) \leq (1-\eta) \cdot 1 + \eta \cdot \exp\left(-\frac{\theta v_t}{\sigma^2}\right) \leq 1 - \eta \left(1 - e^{-\theta \lambda_{\min}/(2\sigma^2)}\right).$$

Consequently,

$$\mathbb{P}_{\text{flip}}(\sigma) \leq \frac{1}{2} \left[1 - \eta \left(1 - e^{-\theta \lambda_{\min}/(2\sigma^2)}\right) \right], \quad \mathbb{P}_{\text{flip}}^{(\delta)}(\sigma) \leq \frac{1}{2} \left[1 - \eta \left(1 - e^{-\theta \lambda_{\min} \delta^2/(2\sigma^2)}\right) \right].$$

Plugging these bounds into Eq.(7), then we obtain

$$p_{i,j} \geq \frac{1}{2} + \frac{\gamma \eta}{4} \left[2 - e^{-\theta \lambda_{\min}/(2\sigma^2)} - e^{-\theta \lambda_{\min} \delta^2/(2\sigma^2)} \right].$$

Using $\mathbb{E}Z = 2\sqrt{mN}(p_{i,j} - \frac{1}{2})$, we arrive at

$$\mathbb{E}[Z(\gamma, \delta, \sigma)] \geq \sqrt{mN} \gamma \frac{\eta}{2} \left[2 - e^{-\theta \lambda_{\min}/(2\sigma^2)} - e^{-\theta \lambda_{\min} \delta^2/(2\sigma^2)} \right].$$

Recalling that $\eta = (1-\theta)^2/(C_4 \kappa^4)$ gives the result for $\rho(\kappa, \theta) = (1-\theta)^2/(2C_4 \kappa^4)$. Since $\theta \in (0, 1)$ is a fixed hyperparameter, it can be tuned to obtain the tightest possible lower bound

$$\mathbb{E}[Z(\gamma, \delta, \sigma)] \geq \sqrt{mN} \gamma \sup_{\theta \in (0, 1)} \left\{ \rho(\kappa, \theta) \left[2 - \exp\left(-\frac{\theta \lambda_{\min}}{2\sigma^2}\right) - \exp\left(-\frac{\theta \lambda_{\min} \delta^2}{2\sigma^2}\right) \right] \right\}.$$

□

Remark 5 (What the sub-Gaussian assumption covers). The Σ -sub-Gaussian assumption strictly generalizes the Gaussian assumption used in Theorem 2 and many non-Gaussian settings that are common in tabular data: 1) bounded/quantized/discrete features (e.g., “gender” or “education” features); and 2) finite mixtures of light-tailed distributions with uniformly bounded covariances (a finite mixture of sub-Gaussians is sub-Gaussian with the worst-component parameter). In conclusion, non-Gaussian distribution with light tails are covered.

F Experimental Details

F.1 Datasets

The datasets used for evaluation are described in Table 8, where # Rows, # Categorical, # Numerical, # Continuous indicate the number of rows, the number of categorical columns, the number of numerical columns, and the number of numerical columns with continuous density function, respectively. # Train and # Test indicate the number of samples in the training and testing set for downstream machine learning tasks, respectively. The **Adult** [4] dataset was extracted from the 1994 Census database, containing 9 categorical and 6 numerical columns. The **Magic** [5] dataset simulates registration of high energy gamma particles in a ground-based atmospheric Cherenkov gamma telescope and consists of one categorical column and 10 numerical columns. The **Shoppers** [26] dataset quantifies online shoppers’ purchasing intentions with 10 categorical columns and 8 numerical columns. The **Default** [38] dataset presents the default payments of credit card clients, including 10 categorical columns and 14 numerical columns. The **Drybean** [16]

dataset provides image information of seven different registered dry beans, comprising one categorical column and 16 numerical columns.

Here, we explicitly distinguish between continuous from integer-valued (discrete) numerical features, rather than conflating “numerical” with “continuous”. As shown in Table 8, the **Adult** and **Default** datasets contain only discrete feature (0 continuous features), while **Magic** and **Drybean** are dominated by continuous features. Therefore, we believe that the selected benchmark datasets provide a sufficiently balanced evaluation across both discrete and continuous data types, supporting the claim that TAB-DRW is applicable to heterogeneous tabular data.

Table 8: Descriptions of datasets used in evaluation.

Name	Domain	# Rows	# Categorical	# Numerical	# Continuous	# Train	# Test	Task
Adult	Society	48,842	9	6	0	32,561	16,281	Classification
Magic	Physics	19,019	1	10	10	17,117	1,902	Classification
Shoppers	Business	12,330	8	10	3	11,097	1,233	Classification
Default	Finance	30,000	10	14	0	27,000	3,000	Classification
Drybean	Biology	13,611	1	16	14	12,249	1,362	Classification

F.2 Metrics

We detail our data fidelity metrics below:

1. **Density** measures the distributional similarity between synthetic and real data. For each numerical column, we compute the Kolmogorov–Smirnov statistic (KST); for each categorical column, we compute the total variation distance (TVD). The per-column scores are then averaged to yield the overall Density score. Higher values indicate closer alignment of marginal distributions.
2. **Corr** evaluates preservation of inter-column relationships. We compute the Pearson correlation coefficient for every pair of columns and report their mean as the Corr score. Larger values indicate more faithful reproduction of real feature dependencies.
3. **C2ST** quantifies statistical indistinguishability between synthetic and real data. A logistic regression model is trained and evaluated on the training and validation sets, both of which contain a mix of real and synthetic data. We then report the complement of the ROC AUC averaged over all validation splits. Higher values indicate that the model cannot distinguish synthetic from real data.
4. **MLE**: assesses downstream machine learning utility on supervised tasks. We train an XGBoost model [7] on synthetic data, then evaluate it on the real testing set, using AUC for the classification task and RMSE for the regression task. Higher MLE scores reflect better machine learning utility of the synthetic data.

Regarding the metric for watermark detectability, we introduce the one-sided **Z-score** defined in (3) and **FPR / TPR**. A larger Z-score indicates stronger alignment with the pseudorandom bits, thus demonstrating better watermark detectability. we synthesize 100 unwatermarked tables with 1K rows (total 100K rows) and perform Monte Carlo simulation to obtain statistics under H_0 . Specifically, for the estimation of empirical critical value (eg. $q_{0.001}$), we conduct the following procedure:

1. Generate 100 unwatermarked tables with 1K rows (100K rows in total) using TabSyn.
2. Bootstrap sampling rows from 100K rows to construct 100K synthetic tables for watermark detection.
3. Set the 100-th order-statistic $Z_{(100)}$ as the threshold.

Then we have $F_{H_0}(Z_{(100)}) \sim \text{Beta}(100, 99901)$. By Clopper-Pearson interval, the estimation procedure above is sufficient to calibrate the critical value $q_{0.001}$, since the realized FPR has a 95% confidence interval of roughly $0.001 \pm 2 \times 10^{-4}$.

Table 9 presents the empirical mean and standard deviation of the alignment count T_i defined in (3) under H_0 and critical values q_α for $\alpha \in \{0.01, 0.005, 0.001\}$.

FPR / TPR denotes the true and false positive rates under the critical value $q_\alpha = 6$. The FPR refers to the probability of incorrectly identifying an unwatermarked table as containing watermark signal, while the TPR refers to the probability of correctly detecting the watermark signal in a watermarked table. Therefore, an FPR / TPR pair of (0.00, 1.00) indicates an effective watermark—no false alarms and complete detection.

Table 9: Results of Monte Carlo simulation on 100 unwatermarked synthetic tables of 1K rows. Each Entry show an empirical estimation (first value) and a theoretical value (second value) under standard assumption in Lemma 3.

Dataset	$\hat{\mu}_{\text{nwm}}/\mu_{\text{nwm}}$	$\hat{\sigma}_{\text{nwm}}/\sigma_{\text{nwm}}$	$\hat{q}_{0.01}/q_{0.01}$	$\hat{q}_{0.005}/q_{0.005}$	$\hat{q}_{0.001}/q_{0.001}$
Adult	0.86/1.00	0.62/0.71	2.34/2.32	2.59/2.57	3.11/3.09
Magic	2.01/2.00	0.87/1.00	2.28/2.32	2.52/2.57	3.03/3.09
Shoppers	2.03/2.00	0.97/1.00	2.51/2.32	2.78/2.57	3.34/3.09
Default	1.42/1.50	0.78/0.87	2.39/2.32	2.64/2.57	3.16/3.09
Drybean	1.77/2.00	0.89/1.00	2.52/2.32	2.78/2.57	3.35/3.09

For TabularMark, we replace our Z-score with the one defined in [45]:

$$Z = \frac{2(n_g - 0.5 n_w)}{\sqrt{n_w}},$$

where n_w is the total number of key cells and n_g is the count within the “green” domain.

F.3 Implementation Details for Data Generator

TabSyn. TabSyn [40] is an architecture designed for high-quality tabular data synthesis. It addresses the challenges of mixed-type features by mapping raw tabular inputs—including numerical, categorical, and other modalities—into a continuous latent space using a customized variational autoencoder (VAE [14]). The VAE employs Transformer-based encoders and decoders to effectively model inter-column dependencies and generate token-level embeddings. In the embedding space, TabSyn leverages a score-based diffusion model with a simplified linear noise schedule, which enables efficient sampling and preserving fidelity to the original data distribution. The combination of autoencoding and latent-space diffusion allows TabSyn to generate diverse and realistic synthetic tabular data with high efficiency and quality.

Implementation in our work. While our experiments are conducted using the TabSyn framework as the generative backbone, we adhere to the implementation in TabWak [46], which is our primary baseline for comparison, to ensure fair and consistent comparison. Specifically, we replace the original score-based diffusion process in TabSyn with DDPM for training and DDIM for sampling. Therefore, our reproduced baseline results (“W/O”) reported in Table 2 are closely aligned with those in Table 1 of TabWak.

The discrepancies between our “W/O” results and those reported in the original TabSyn paper [40] stem from the two modifications mentioned above. As reported in the TabSyn paper itself, the original score-based TabSyn model outperformed the TabSyn-DDPM variant in generation quality owing to its tailored diffusion process in continuous latent space. Additionally, the deterministic nature of the DDIM sampler may reduce data diversity compared to the original score-based SDE sampler. Nevertheless, the DDIM sampler is essential for TabWak, as its watermark detection relies on the inversion process.

In Table 10, we also present the evaluation results of our methods on synthetic tabular data generated by original TabSyn implementation. See Appendix G.1 for more empirical results and analysis.

F.4 Implementation Details for Watermarking

Our method. We sample half of the column indices using a secret key to form the index set \mathcal{I} in Algorithm 3. The selection of hyperparameter λ in YJT is implemented by the Python module `scipy.stats.yeojohnson` [27]. For the Adult, Magic and Drybean datasets, we apply Algorithm 1 to all numerical columns. For the Shoppers dataset, we apply watermarking to first 9 numerical columns. For the Default dataset, we select columns $\{0, 4, 17, 18, 19, 20, 21, 22\}$ for watermarking. We provide explanations on this implementation details in Remark 2.

MUSE. Following the experimental setting in [8], we adopt Bernoulli as the scoring function and an adaptive column selection mechanism with three columns. We also adhere to the original configuration of $m = 2$, meaning that between two candidate rows, the one with the higher score is selected as the watermarked sample. Since TabSyn generates tabular data as a whole rather than row by row, we generate twice the target number of rows and then perform selection, consistent with the workflow illustrated in Algorithm 1 of [8].

TabWak*. We rigorously reproduce TabWak* with valid bit mechanism by following all instructions provided in the official repository <https://github.com/chaoyitud/TabWak>. However, we observed a significant discrepancy between our reproduction results and those reported in the original TabWak paper [46]. Below, we clarify the source of this discrepancy.

In TabWak’s detection pipeline, the suspect tabular data \mathbf{X} is first mapped into a continuous latent space via the inversion of the VAE decoder to obtain an initial latent representation \mathbf{z}_0 . This is then passed through DDIM inversion to recover the watermarked representation \mathbf{z}_T . In practice, TabWak codebase obtains \mathbf{z}_0 from \mathbf{X} by solving a gradient-based optimization problem to approximate the inversion of the VAE decoder, which is formulated as:

$$\mathbf{z} = \arg \min_{\mathbf{z}} \|\mathbf{x} - f_{\theta}(\mathbf{z})\|_2,$$

where f_{θ} denotes the trained VAE decoder.

However, we found that the optimization procedure often fails to converge to the true latent code \mathbf{z}_0 , which leads to significantly reduced detectability and robustness of the watermark signal (as reported in our paper). We also note that in the official TabWak codebase, the ground-truth \mathbf{z}_0 is saved during generation. Using this saved \mathbf{z}_0 bypasses the inversion step and yields strong detectability, which is comparable to that reported in the original TabWak paper. But this approach is impractical in real-world detection where the ground-truth \mathbf{z}_0 is unavailable.

GLW. We set the number of “green list” intervals to $m = 5$. Since GLW was originally designed for tabular data with continuous density functions, we introduce a minor modification to extend it to mixed-type tabular data. Specifically, for entries with non-zero decimal components, we directly apply the standard method proposed in [11]. For integer entries with non-zero units digits, we shift the decimal point one place to the left, apply the method to the transformed values, and then shift them back. To prevent significant distortion, we exclude entries with absolute values less than 1 from watermarking. GLW is applied to all numerical columns across all datasets.

TabularMark. Following the original experimental setup, we select the first numerical column as the watermark attribute, from which 10% of the cells are pseudorandomly chosen as key cells. The perturbation range p is set to 25, and the number of unit domains k to 500. To implement the matching algorithm in [45], we extract the first five binary bits from each of five randomly selected attributes and concatenate them to form a 25-bit binary string, which serves as the primary key for each tuple.

F.5 Implementation Details for Tabular Attacks

We implement the ten post-processing attacks for Table 3 as below:

1. **Row Del.** removes 10% of rows in a table.
2. **Col Del.** replaces 2 columns with unwatermarked values sampled from the same model.
3. **Cell Del.** replaces 10% cells with unwatermarked values sampled from the same model.
4. **Gaussian-Noise.** adds Gaussian noise with zero mean and a standard deviation equal to 10% of each cell’s value for numerical attributes.
5. **Categorical-Noise.** perturbs categorical entries by randomly replacing 10% of cells with values sampled from other rows in the same column.
6. **A(daptive)-Noise.** adds Gaussian noise with zero mean and 0.1 standard deviation to standardized attributes. Specifically, we conduct the process below for each column $j \in \{1, \dots, p\}$:

$$z_{ij} = \frac{x_{ij} - \mu_j}{\sigma_j}, \quad z'_{ij} = z_{ij} + \epsilon \cdot \mathcal{N}(0, 1), \quad x'_{ij} = z'_{ij} \cdot \sigma_j + \mu_j,$$

where $\epsilon = 0.1$ is the attack strength, and μ_j and σ_j are the empirical mean and standard deviation of column j in the original data. Conducting round and clip if x'_{ij} is not in the valid range of column j in the original data.

7. **Truncation.** truncates numerical values at the first significant digit.
8. **Quantization.** discretizes numerical columns using quantile transformation with the 10 quantile bins and maps those discrete quantile levels back to the original data domain with the inverse transform.
9. **Resample.** redistributes samples to achieve equal representation across target classes by super-sampling underrepresented classes and sub-sampling overrepresented ones.
10. **Shuffle.** randomly permutes all rows of the table.

Table 10: Data fidelity and watermark detectability evaluated on tables generated by original TabSyn implementation. No watermarking is denoted as “W/O”. Our proposed TAB-DRW uses $(\gamma, \delta) = (0.5, 0.5)$. Fidelity metrics are averaged over 10 trials while Z-score is averaged over 100 trials.

Datasets	Method	Fidelity Metric				Z-score	
		Density \uparrow	Corr \uparrow	C2ST \uparrow	MLE \uparrow	1k rows \uparrow	5k rows \uparrow
Adult	W/O	0.993 \pm 0.001	0.982 \pm 0.003	0.994 \pm 0.001	0.912 \pm 0.002	–	–
	TAB-DRW	0.981 \pm 0.004	0.967 \pm 0.003	0.988 \pm 0.006	0.910 \pm 0.003	12.57 \pm 1.16	28.07 \pm 0.99
Magic	W/O	0.990 \pm 0.001	0.991 \pm 0.003	0.993 \pm 0.002	0.936 \pm 0.002	–	–
	TAB-DRW	0.983 \pm 0.003	0.978 \pm 0.003	0.991 \pm 0.004	0.933 \pm 0.002	27.11 \pm 0.77	61.02 \pm 0.82
Shoppers	W/O	0.985 \pm 0.003	0.973 \pm 0.002	0.964 \pm 0.003	0.920 \pm 0.005	–	–
	TAB-DRW	0.976 \pm 0.005	0.955 \pm 0.003	0.953 \pm 0.007	0.919 \pm 0.006	17.30 \pm 1.02	39.31 \pm 1.06
Default	W/O	0.987 \pm 0.001	0.952 \pm 0.001	0.975 \pm 0.002	0.764 \pm 0.004	–	–
	TAB-DRW	0.982 \pm 0.002	0.948 \pm 0.004	0.971 \pm 0.009	0.764 \pm 0.005	16.87 \pm 0.91	37.73 \pm 0.88
Drybean	W/O	0.987 \pm 0.002	0.992 \pm 0.003	0.978 \pm 0.003	0.911 \pm 0.006	–	–
	TAB-DRW	0.984 \pm 0.004	0.977 \pm 0.007	0.972 \pm 0.006	0.908 \pm 0.009	41.23 \pm 0.98	90.33 \pm 1.06

While additive Gaussian noise (G-noise) attack adopted in our paper may destroy semantic meanings of columns with large absolute values and very small variance, we adhere to it for two main reasons. First, this ensures a fair comparison of robustness with TabWak* by replicating the evaluation setup used in its original paper [46]. Second, if our watermark signal remains highly detectable under such strong attacks that may significantly distort data utility, it is reasonable to expect stronger performance under milder perturbations. In fact, adaptive Gaussian noise (A-Noise) attack is implemented as a milder variant of Gaussian noise attack.

Additionally, although all the watermark methods including ours show great robustness to the shuffling attack, we believe that the shuffle attack should not be omitted. In practice, the existence of this cost-free row-level attack has important implications for our design. Without shuffle attack, we could use the record indices as hash seeds to deterministically sample pseudorandom bit sequences for each row, enabling accurate recovery during detection and avoiding key collision. However, the bit sequence recovery becomes vulnerable when row-ordering is no longer preserved under shuffle attack.

We do not include the column-level shuffle attack, since table owners or model providers can easily recover the original column order using headers, statistical properties, or semantic features of the columns before watermark detection.

In Appendix G.3, we present extended robustness evaluations against above attacks with higher strength.

G Additional Results and Analysis

G.1 Ablation Study

Model-agnostic property. Table 10 presents the evaluation results of TAB-DRW on TabSyn implemented using the official codebase. The empirical results show the effectiveness of our method on high-fidelity synthetic data, further justifying our claim that TAB-DRW is practical and the fidelity-detectability trade-off only relies on the hyperparameters.

While our experiments are conducted using TabSyn framework as the generative backbone, we expect TAB-DRW to exhibit similar performance when applied to other synthetic tabular data generators, since TAB-DRW is a post-editing watermarking method that operates independently of the generative model’s architecture or sampling procedure.

To justify this claim, we perform evaluations using two additional popular tabular data generators: TabDDPM [17] and STaSy [13]. The results are presented in Table 11. Overall, our method achieves great fidelity-detectability trade-off across all three models (including TabSyn), demonstrating its effectiveness and model-agnostic property.

YJT selection. In TAB-DRW, the Yeo-Johnson transformation (YJT) serves as a pre-conditioner for constructing the frequency-domain representation. By mapping each feature toward a more Gaussian-like distribution, YJT helps to standardize heterogeneous feature scales and reduce skewness, which is essential for enabling a stable, low-distortion watermarking process in the frequency domain.

Table 11: Data fidelity and watermark detectability evaluated on tables generated by TabDDPM and STaSy. For fidelity metrics, the first value in each entry denotes the result without watermark, while the second value denotes the result of TAB-DRW with $(\gamma, \delta) = (0.5, 0.5)$.

Datasets	Model	Fidelity Metric				Z-score	
		Density \uparrow	Corr \uparrow	C2ST \uparrow	MLE \uparrow	1k rows \uparrow	5k rows \uparrow
Adult	TabDDPM	0.982/0.967	0.969/0.958	0.975/0.973	0.903/0.894	12.44 \pm 0.96	29.07 \pm 1.05
	STaSy	0.887/0.883	0.864/0.858	0.408/0.423	0.901/0.893	13.07 \pm 1.22	29.95 \pm 1.19
Magic	TabDDPM	0.989/0.971	0.983/0.975	0.999/0.996	0.935/0.923	28.74 \pm 0.98	62.53 \pm 1.14
	STaSy	0.937/0.927	0.933/0.919	0.694/0.688	0.933/0.926	27.95 \pm 0.89	61.48 \pm 0.97
Shoppers	TabDDPM	0.972/0.959	0.933/0.921	0.834/0.832	0.918/0.911	17.94 \pm 1.24	39.27 \pm 1.22
	STaSy	0.906/0.898	0.915/0.907	0.548/0.553	0.914/0.908	17.49 \pm 1.06	38.52 \pm 1.17
Default	TabDDPM	0.985/0.982	0.951/0.948	0.971/0.967	0.756/0.755	15.27 \pm 0.94	35.29 \pm 0.92
	STaSy	0.942/0.940	0.940/0.939	0.681/0.677	0.752/0.749	16.65 \pm 1.00	37.02 \pm 1.14
Drybean	TabDDPM	0.987/0.984	0.971/0.960	0.967/0.954	0.892/0.894	40.22 \pm 1.16	88.59 \pm 0.94
	STaSy	0.949/0.947	0.919/0.912	0.582/0.596	0.890/0.891	39.47 \pm 1.05	86.98 \pm 0.91

Table 12: Ablation study on YJT. Both methods are applied to TAB-DRW with $(\gamma, \delta) = (0.5, 0.5)$. Fidelity metrics are averaged over 10 trials while Z-score is averaged over 100 trials.

Datasets	Method	Fidelity Metric				Z-score	
		Density \uparrow	Corr \uparrow	C2ST \uparrow	MLE \uparrow	1k rows \uparrow	5k rows \uparrow
Adult	W/O YJT	0.906 \pm 0.004	0.862 \pm 0.003	0.601 \pm 0.006	0.812 \pm 0.007	13.74\pm0.87	31.62\pm0.95
	W/ YJT	0.915\pm0.005	0.864\pm0.004	0.604\pm0.008	0.816\pm0.009	12.81 \pm 1.17	29.55 \pm 1.12
Magic	W/O YJT	0.907 \pm 0.004	0.936\pm0.003	0.666 \pm 0.002	0.817 \pm 0.011	27.17 \pm 0.95	60.91 \pm 0.93
	W/ YJT	0.910\pm0.005	0.935 \pm 0.003	0.676\pm0.009	0.818\pm0.014	27.34\pm0.93	61.42\pm1.02
Shoppers	W/O YJT	0.896 \pm 0.005	0.900 \pm 0.002	0.704 \pm 0.009	0.888 \pm 0.012	12.79 \pm 0.96	28.50 \pm 0.98
	W/ YJT	0.909\pm0.006	0.902\pm0.003	0.712\pm0.013	0.891\pm0.014	18.18\pm1.28	40.74\pm1.26
Default	W/O YJT	0.921 \pm 0.007	0.906 \pm 0.008	0.689 \pm 0.014	0.789 \pm 0.011	10.05 \pm 0.98	22.73 \pm 1.08
	W/ YJT	0.929\pm0.010	0.907\pm0.011	0.713\pm0.018	0.791\pm0.013	15.98\pm0.92	35.84\pm0.91
Drybean	W/O YJT	0.923 \pm 0.009	0.911 \pm 0.004	0.527 \pm 0.016	0.877 \pm 0.014	28.12 \pm 0.87	62.80 \pm 0.79
	W/ YJT	0.931\pm0.013	0.928\pm0.007	0.655\pm0.029	0.880\pm0.019	38.03\pm1.03	85.05\pm0.67

We further emphasize that YJT also improves the robustness of rank-based statistics used in our pseudorandom bit generation procedure. Specifically, transforming the feature distributions makes ranks more evenly spread and less sensitive to local density variations, which in turn improves bit consistency under post-processing perturbations.

To support this claim empirically, we include an ablation study comparing TAB-DRW with and without YJT. As shown in the Table 12, the YJT consistently yields a better trade-off between fidelity and watermark detectability, confirming its importance in our design.

Gray code selection. We provide additional experimental results using a 1-Gray code and compare it to our adopted variant of 2-Gray code. Specifically, we modify lines 7 and 9 in Algorithm 3 as follows: We change line 7 to “**for** $j \leftarrow 1$ **to** m **do**” and line 9 to “Append 1 to S if $k \% 4 = 0$ or 3; otherwise append 0”. We set the attack strengths for robustness evaluation the same as the strengthened version adopted in Appendix G.3.

From the results, we observe that using a 1-Gray code for bit generation yields a slight improvement in data fidelity, as it more closely mimics an ideal bit sampled from a Bernoulli distribution. However, its detectability and robustness decrease on several datasets, especially those dominated by continuous variables such as **Magic** and **Drybean**. We attribute this to the finer-grained rank-bin partition induced by the 1-Gray code and to the greater instability of the sum-based score for continuous features under perturbations, which makes cross-bin rank shifts more likely to happen.

Table 13: Data fidelity and watermark detectability evaluated on TAB-DRW using different Gray codes for bit generation. Fidelity metrics are averaged over 10 trials while Z-scores are averaged over 100 trials.

Datasets	Bit Gen.	Fidelity Metric				Z-score	
		Density \uparrow	Corr \uparrow	C2ST \uparrow	MLE \uparrow	1k rows \uparrow	5k rows \uparrow
Adult	1-Gray code	0.916 \pm 0.005	0.863 \pm 0.005	0.600 \pm 0.009	0.816 \pm 0.008	11.06 \pm 0.99	24.95 \pm 0.86
	2-Gray code	0.915 \pm 0.005	0.864 \pm 0.004	0.604 \pm 0.008	0.816 \pm 0.009	12.81 \pm 1.17	29.55 \pm 1.12
Magic	1-Gray code	0.917 \pm 0.006	0.936 \pm 0.003	0.676 \pm 0.008	0.818 \pm 0.014	21.74 \pm 0.96	48.78 \pm 0.97
	2-Gray code	0.917 \pm 0.005	0.937 \pm 0.003	0.676 \pm 0.009	0.818 \pm 0.014	27.34 \pm 0.93	61.42 \pm 1.02
Shoppers	1-Gray code	0.909 \pm 0.006	0.909 \pm 0.004	0.715 \pm 0.011	0.892 \pm 0.014	17.30 \pm 1.14	38.48 \pm 1.14
	2-Gray code	0.909 \pm 0.006	0.902 \pm 0.003	0.712 \pm 0.013	0.891 \pm 0.014	18.18 \pm 1.28	40.74 \pm 1.26
Default	1-Gray code	0.927 \pm 0.010	0.918 \pm 0.009	0.715 \pm 0.013	0.793 \pm 0.013	15.07 \pm 1.02	33.72 \pm 0.97
	2-Gray code	0.929 \pm 0.010	0.907 \pm 0.011	0.717 \pm 0.018	0.791 \pm 0.013	15.98 \pm 0.92	35.84 \pm 0.91
Drybean	1-Gray code	0.933 \pm 0.010	0.932 \pm 0.007	0.659 \pm 0.022	0.880 \pm 0.019	25.40 \pm 0.92	57.74 \pm 1.03
	2-Gray code	0.931 \pm 0.013	0.928 \pm 0.007	0.655 \pm 0.029	0.880 \pm 0.019	38.03 \pm 1.03	85.05 \pm 0.67

Table 14: Robustness evaluation of TAB-DRW using different Gray codes for bit generation under the strengthened attack setting. Z-scores are averaged over 100 trials on tables with 5k rows.

Datasets	Bit Gen.	Attacks									
		Row Del.	Col Del.	Cell Del.	G-Noise	C-Noise	A-Noise	Truncation	Quantization	Resample	Shuffle
Adult	1-Gray code	22.30	10.10	11.19	12.32	18.11	21.24	24.95	16.04	21.49	24.95
	2-Gray code	26.34	13.12	14.37	14.29	20.10	21.85	29.55	16.41	28.15	29.55
Magic	1-Gray code	43.47	8.46	16.27	22.81	44.14	21.42	38.83	19.32	24.58	48.78
	2-Gray code	54.85	11.75	21.60	33.93	48.38	29.06	52.62	26.43	37.61	61.42
Shoppers	1-Gray code	34.36	13.40	14.00	35.54	25.05	13.12	31.00	23.36	14.34	38.48
	2-Gray code	36.21	13.75	13.27	37.71	32.60	13.10	30.28	25.72	29.28	40.74
Default	1-Gray code	29.84	19.45	15.05	21.66	26.14	12.52	33.72	11.06	30.08	33.72
	2-Gray code	31.92	20.70	15.44	23.75	27.20	16.99	35.84	14.10	32.36	35.84
Drybean	1-Gray code	51.38	15.48	16.87	12.73	48.93	15.50	22.94	15.31	39.44	57.74
	2-Gray code	75.91	32.92	35.27	23.57	77.70	42.48	42.14	45.95	68.69	85.05

Table 15: Data fidelity and watermark detectability evaluated on TAB-DRW with different columns selected for watermarking. Fidelity metrics are averaged over 10 trials, and Z-scores are averaged over 100 trials.

Datasets	Col. Selection	Fidelity Metric				Z-score			
		Density \uparrow	Corr \uparrow	C2ST \uparrow	MLE \uparrow	1k rows \uparrow	5k rows \uparrow		
Adult	All Col.	0.909 \pm 0.005	0.859 \pm 0.005	0.597 \pm 0.009	0.808 \pm 0.008	14.56 \pm 0.99	32.89 \pm 1.06		
	Original	0.915 \pm 0.005	0.864 \pm 0.004	0.604 \pm 0.008	0.816 \pm 0.009	12.81 \pm 1.17	29.55 \pm 1.12		
Magic	All Col.	0.914 \pm 0.006	0.936 \pm 0.003	0.674 \pm 0.008	0.818 \pm 0.014	24.66 \pm 1.08	55.47 \pm 1.09		
	Original	0.917 \pm 0.005	0.937 \pm 0.003	0.676 \pm 0.009	0.818 \pm 0.014	27.34 \pm 0.93	61.42 \pm 1.02		
Shoppers	All Col.	0.901 \pm 0.005	0.897 \pm 0.003	0.704 \pm 0.009	0.887 \pm 0.012	19.59 \pm 1.08	43.84 \pm 1.14		
	Original	0.909 \pm 0.006	0.902 \pm 0.003	0.712 \pm 0.013	0.891 \pm 0.014	18.18 \pm 1.28	40.74 \pm 1.26		
Default	All Col.	0.919 \pm 0.009	0.902 \pm 0.013	0.705 \pm 0.019	0.787 \pm 0.011	22.21 \pm 1.03	49.96 \pm 0.99		
	Original	0.929 \pm 0.010	0.907 \pm 0.011	0.717 \pm 0.018	0.791 \pm 0.013	15.98 \pm 0.92	35.84 \pm 0.91		
Drybean	All Col.	0.929 \pm 0.010	0.924 \pm 0.007	0.649 \pm 0.022	0.878 \pm 0.019	38.35 \pm 0.89	85.47 \pm 0.73		
	Original	0.931 \pm 0.013	0.928 \pm 0.007	0.655 \pm 0.029	0.880 \pm 0.019	38.03 \pm 1.03	85.05 \pm 0.67		

Column selection for watermarking. In the main paper, our empirical evaluation focuses on numerical columns (including mixed continuous and discrete types) to enable a fair comparison with the other post-editing watermarking methods, GLW and TabularMark, which both suffer substantial fidelity degradation when applied to all columns. Here we also report results obtained by applying TAB-DRW to all columns, showing how different selection strategies influence the tradeoff between fidelity and detectability. In general, using more columns for watermarking improves robustness (Theorem 2 shows that the lower bound of the Z-score scales with the number of selected columns), while

Table 16: Detection performance of TAB-DRW with or without the rounding and clipping operations. Z-scores are averaged over 100 trials on tables with 1k rows. “Rounding magnitude” denotes the average rounding magnitude of discrete entries, and “Clipping ratio” denotes the fraction of discrete entries that are clipped.

Dataset	W/O round and clip	W/ round and clip	Rounding magnitude	Clipping ratio
Adult	15.21 ± 1.00	12.81 ± 1.17	0.0911 ± 0.0015	0.0008 ± 0.0004
Magic	27.34 ± 0.93	27.34 ± 0.93	0.0000 ± 0.0000	0.0000 ± 0.0000
Shoppers	21.00 ± 1.15	18.18 ± 1.28	0.0969 ± 0.0042	0.0244 ± 0.0036
Default	17.94 ± 0.95	15.98 ± 0.92	0.0542 ± 0.0018	0.0151 ± 0.0013
Drybean	37.79 ± 1.02	38.03 ± 1.03	0.1285 ± 0.0027	0.0145 ± 0.0022

Table 17: Comparison of watermark embedding runtimes (in seconds) across methods. For each entry, the first value indicates the total GPU time to generate a 1K-row watermarked table with TabSyn, and the second value denotes the watermark embedding CPU time for an existing 1K-row table.

Dataset	GLW	MUSE	TabWak*	TabularMark	TAB-DRW
Adult	$1.896(0.031)$	$3.878(0.593)$	$1.904(-)$	$1.896(0.008)$	$1.896(0.112)$
Magic	$1.897(0.026)$	$3.963(0.555)$	$1.893(-)$	$1.897(0.007)$	$1.897(0.106)$
Shoppers	$1.912(0.026)$	$3.938(0.629)$	$1.932(-)$	$1.912(0.008)$	$1.912(0.142)$
Default	$1.925(0.052)$	$4.114(0.688)$	$1.945(-)$	$1.925(0.009)$	$1.925(0.205)$
Drybean	$1.920(0.025)$	$3.967(0.601)$	$1.936(-)$	$1.920(0.009)$	$1.920(0.152)$

Table 18: Comparison of watermark detection runtimes (in seconds) on 1K-row watermarked table across watermarking methods. Values for TabWak* denote GPU runtimes, whereas all other methods are measured in CPU time.

Dataset	GLW	MUSE	TabWak*	TabularMark	TAB-DRW
Adult	0.003	0.177	27.96	0.717	0.100
Magic	0.001	0.161	21.78	0.729	0.076
Shoppers	0.005	0.188	30.27	0.682	0.106
Default	0.004	0.234	35.49	0.713	0.152
Drybean	0.003	0.193	26.03	0.582	0.120

incurring slightly higher distortion. The results in Table 15 show that watermarking more columns improves detectability while reducing fidelity, consistent with our theoretical analysis.

Impact of rounding and clipping on watermark detectability. Since the outputs of the inverse DFT and YJT are real-valued, rounding and clipping are necessary for discrete features to preserve semantic validity. However, these operations may also perturb the sign-bit alignment in the frequency domain, potentially weakening the watermark signal. Fortunately, the sign-bit alignment of TAB-DRW is highly insensitive to such mild nonlinear perturbations. In addition, because our method preserves fidelity well under appropriate choices of (γ, δ) , clipping occurs only rarely and rounding magnitudes remain minimal.

Table 16 shows the results of an ablation study comparing Z-scores with and without rounding and clipping across five datasets, together with the frequency and magnitude of these operations. For **Magic** dataset there are no rounding or clipping happening since all the columns are continuous. For other datasets, the impact of these two post-processing operations on watermark detectability is negligible.

G.2 Runtime Evaluation

Tables 17 and 18 report the average runtimes for watermark embedding and detection on five benchmark datasets. Each result is averaged over 100 independent trials on synthetic tabular data with 1K rows. We run the experiments on a M1 Pro CPU and a 40GB NVIDIA A100 GPU.

Table 19: Comparison of watermark detection runtimes (in seconds) on 100K-row watermarked table across watermarking methods. Values for TabWak* denote GPU runtimes, whereas all other methods are measured in CPU time.

Dataset	GLW	MUSE	TabWak*	TabularMark	TAB-DRW
Adult	0.20	14.61	1808.60	80.69	2.05
Magic	0.10	13.06	1472.28	71.89	2.02
Shoppers	0.31	15.76	1659.47	89.42	3.12
Default	0.38	17.91	1994.51	87.85	3.88
Drybean	0.15	16.63	1569.88	82.37	2.87

Table 20: Watermark robustness against attacks with higher strength. Average Z-score on 5k rows under seven variable-strength attacks. Each value is obtained by repeating the attacks 100 times (10 times for “TabWak*”) and averaging the results. Our proposed TAB-DRW is evaluated with the hyperparameter $(\gamma, \delta) = (0.5, 0.5)$. Best performances are shown in **bold**, and second-best are underlined.

Datasets	Method	Attacks						
		Row Del.	Col Del.	Cell Del.	G-Noise	C-Noise	A-Noise	Quantization
		20%	3 col	20%	20%	20%	20%	20%
Adult	GLW	14.76	13.10	<u>13.19</u>	0.00	<u>16.54</u>	2.77	3.03
	MUSE	13.31	4.96	<u>6.17</u>	<u>11.84</u>	<u>8.05</u>	3.99	<u>10.99</u>
	TabWak*	14.44	8.05	7.87	0.02	15.67	<u>10.23</u>	5.56
	TabularMark	<u>20.29</u>	13.92	12.99	3.31	5.54	0.62	0.00
	TAB-DRW	26.34	<u>13.12</u>	14.37	14.29	20.10	21.85	16.41
Magic	GLW	153.98	123.60	137.64	0.10	172.20	0.31	<u>14.08</u>
	MUSE	31.56	3.70	9.30	8.39	33.34	4.06	0.39
	TabWak*	17.27	7.47	13.45	<u>16.44</u>	19.76	<u>13.39</u>	12.86
	TabularMark	16.09	10.68	11.74	0.00	19.39	0.68	0.00
	TAB-DRW	<u>54.85</u>	<u>11.75</u>	<u>21.60</u>	33.93	48.38	29.06	26.43
Shoppers	GLW	36.82	34.46	32.33	0.00	39.08	1.13	0.00
	MUSE	25.85	8.64	9.05	<u>21.58</u>	16.20	16.26	<u>13.61</u>
	TabWak*	8.93	2.26	0.97	0.00	10.47	1.22	0.69
	TabularMark	13.68	8.74	10.13	0.98	13.29	0.00	1.42
	TAB-DRW	<u>36.21</u>	<u>13.75</u>	<u>13.27</u>	37.71	32.60	<u>13.10</u>	25.72
Default	GLW	25.67	<u>19.89</u>	19.88	0.00	<u>27.08</u>	6.49	9.60
	MUSE	30.80	8.52	7.30	14.01	17.67	3.79	4.97
	TabWak*	21.96	12.84	13.49	23.77	23.70	18.52	20.25
	TabularMark	19.72	16.21	11.17	0.00	17.10	0.80	2.58
	TAB-DRW	31.92	20.70	<u>15.44</u>	<u>23.75</u>	27.20	<u>16.99</u>	<u>14.10</u>
Drybean	GLW	116.96	104.46	98.54	0.18	123.28	5.05	<u>27.90</u>
	MUSE	28.12	4.58	6.34	6.13	27.71	2.85	0.00
	TabWak*	16.01	0.00	0.00	<u>11.21</u>	17.53	<u>10.42</u>	3.43
	TabularMark	12.06	5.27	3.22	0.00	13.54	2.43	0.00
	TAB-DRW	<u>75.91</u>	<u>32.92</u>	<u>35.27</u>	23.57	77.70	42.48	45.95

Among all compared methods, MUSE incurs the highest embedding cost, as it selects the highest-scoring row from multiple candidates, thereby requiring the generation of multiple unwatermarked samples. By contrast, TabWak* imposes the highest detection cost, since it embeds watermarks in the latent space of a large diffusion model and relies on the DDIM inversion process for detection, which demands GPU resources for tensor acceleration. In contrast, post-editing approaches such as GLW, TabularMark, and our proposed TAB-DRW embed and detect watermarks after table generation, without accessing the generative pipeline. These methods are significantly more efficient—achieving detection speeds several orders of magnitude faster than TabWak*—and can be executed entirely on CPU without loss of performance.

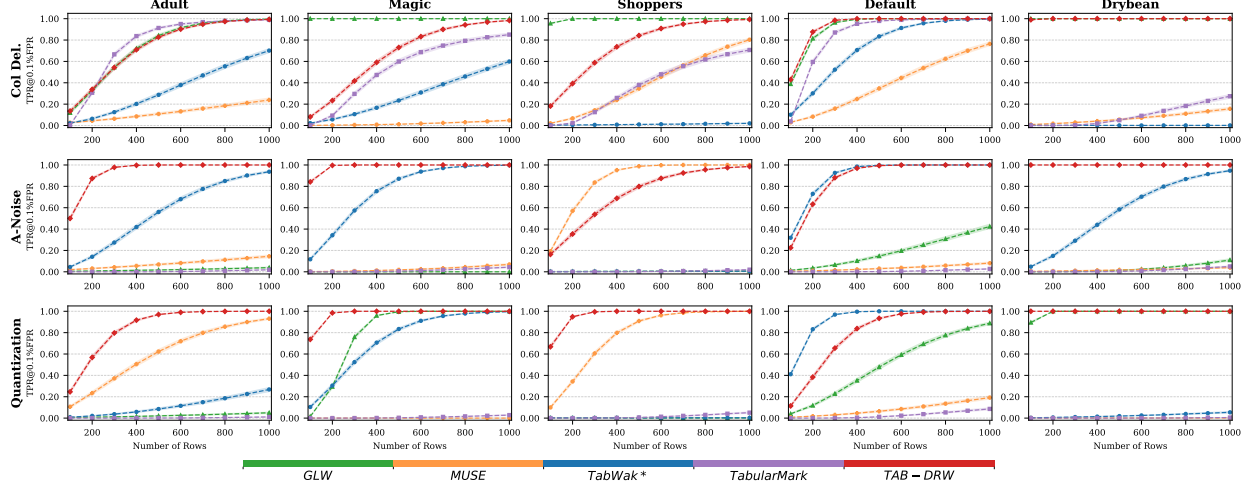


Figure 8: TPR@0.1%FPR versus row count under three representative attacks with higher strength. Dashed lines show the bootstrap mean estimate (500 resamples), and shaded regions indicate the 90% confidence interval.

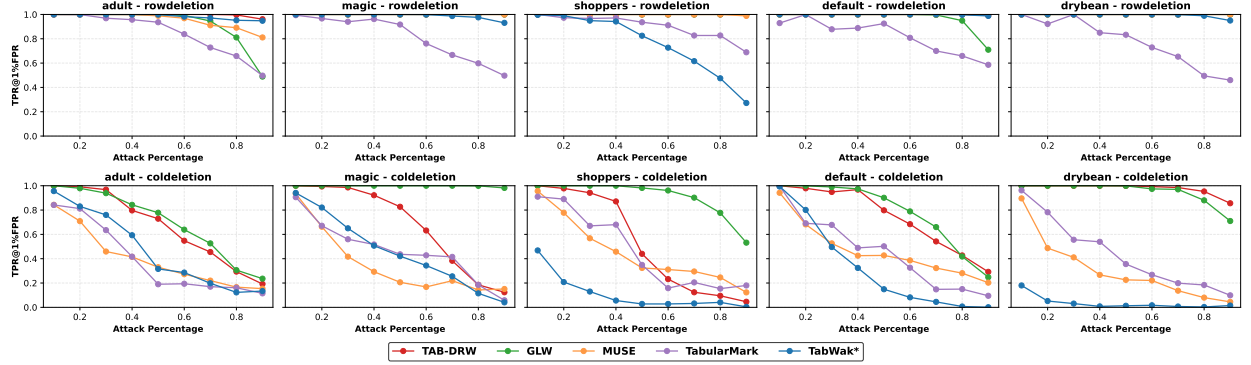


Figure 9: TPR@1%FPR versus attack strength under row and column deletion attacks. All experiments are conducted on tables with 1K rows. Each value denotes the result of 100 independent trials.

As shown in Tables 17, 18, and 19, once unwatermarked samples are generated, the grid search tuning described in Section 2 can be applied to the synthetic data with negligible overhead—on the order of seconds for datasets comparable in scale to our benchmarks—and can be executed entirely on CPU.

G.3 Additional Robustness Evaluation

Post-processing attacks with high strength. In this section, we benchmark the robustness of TAB-DRW and other watermarking methods using attacks with higher strength. Specifically, we use the setting below:

1. **Row Del.** removes 20% of rows in a table.
2. **Col Del.** replaces 3 columns with unwatermarked values sampled from the same model.
3. **Cell Del.** replaces 20% cells with unwatermarked values sampled from the same model.
4. **Gaussian-Noise.** adds Gaussian noise with zero mean and a standard deviation equal to 20% of each cell’s value for numerical attributes.
5. **Categorical-Noise.** perturbs categorical entries by randomly replacing 20% of cells with values sampled from other rows in the same column.
6. **A(daptive)-Noise.** adds Gaussian noise with zero mean and 0.2 standard deviation to standardized attributes.
7. **Quantization.** discretizes numerical columns using quantile transformation with the 10 quantile bins and maps those discrete quantile levels back to the original data domain with the inverse transform.

Table 21: Data fidelity and watermark detectability of privacy-enhanced TAB-DRW under varying watermark keys. All experiments use $(\gamma, \delta) = (0.5, 0.5)$. Fidelity metrics are averaged over 10 trials, and the Z -score is averaged over 100 trials.

Datasets	Key	Fidelity Metric				Z-score	
		Density \uparrow	Corr \uparrow	C2ST \uparrow	MLE \uparrow	1k rows \uparrow	5k rows \uparrow
Adult	W/O	0.922 \pm 0.001	0.872 \pm 0.001	0.611 \pm 0.004	0.824 \pm 0.005	–	–
	Key 48	0.912 \pm 0.003	0.862 \pm 0.003	0.598 \pm 0.008	0.814 \pm 0.009	11.98 \pm 0.97	26.48 \pm 1.07
	Key 496	0.916\pm0.003	0.869\pm0.004	0.601 \pm 0.006	0.819\pm0.009	16.69\pm1.24	37.39\pm1.37
	Key 928	0.915 \pm 0.005	0.864 \pm 0.004	0.604\pm0.008	0.816 \pm 0.009	12.81 \pm 1.17	29.55 \pm 1.12
Magic	W/O	0.917 \pm 0.001	0.945 \pm 0.003	0.672 \pm 0.004	0.823 \pm 0.007	–	–
	Key 48	0.915\pm0.004	0.934 \pm 0.005	0.676\pm0.009	0.821\pm0.009	24.06 \pm 0.75	53.19 \pm 0.86
	Key 496	0.915 \pm 0.004	0.939\pm0.005	0.666 \pm 0.007	0.819 \pm 0.012	27.33 \pm 1.04	61.17 \pm 1.08
	Key 928	0.910 \pm 0.005	0.935 \pm 0.003	0.676 \pm 0.009	0.818 \pm 0.014	27.34\pm0.93	61.42\pm1.02
Shoppers	W/O	0.919 \pm 0.002	0.910 \pm 0.001	0.704 \pm 0.005	0.902 \pm 0.012	–	–
	Key 48	0.912\pm0.004	0.907\pm0.002	0.706 \pm 0.008	0.893\pm0.015	16.15 \pm 1.11	36.11 \pm 1.16
	Key 496	0.904 \pm 0.005	0.902 \pm 0.003	0.698 \pm 0.011	0.889 \pm 0.015	14.84 \pm 1.10	34.28 \pm 1.16
	Key 928	0.909 \pm 0.006	0.902 \pm 0.003	0.712\pm0.013	0.891 \pm 0.014	18.18\pm1.28	40.74\pm1.26
Default	W/O	0.930 \pm 0.001	0.907 \pm 0.001	0.717 \pm 0.003	0.797 \pm 0.009	–	–
	Key 48	0.929\pm0.010	0.906 \pm 0.007	0.715\pm0.010	0.791\pm0.013	13.56 \pm 1.02	30.32 \pm 0.98
	Key 496	0.929 \pm 0.010	0.907\pm0.010	0.714 \pm 0.012	0.791 \pm 0.013	13.82 \pm 0.96	30.90 \pm 0.99
	Key 928	0.929 \pm 0.010	0.907 \pm 0.011	0.713 \pm 0.018	0.791 \pm 0.013	15.98\pm0.92	35.84\pm0.91
Drybean	W/O	0.932 \pm 0.001	0.935 \pm 0.001	0.640 \pm 0.003	0.878 \pm 0.009	–	–
	Key 48	0.930 \pm 0.007	0.926 \pm 0.005	0.649 \pm 0.014	0.881\pm0.017	37.21 \pm 0.84	83.14 \pm 0.91
	Key 496	0.930 \pm 0.007	0.929\pm0.006	0.631 \pm 0.025	0.875 \pm 0.011	30.98 \pm 0.91	70.27 \pm 0.83
	Key 928	0.931\pm0.013	0.928 \pm 0.007	0.655\pm0.029	0.880 \pm 0.019	38.03\pm1.03	85.05\pm0.67

Since the **Truncation**, **Resample**, and **Shuffle** attacks are applied with fixed strength, we omit them here.

Table 20 reports the average one-sided Z -score over 5k rows, evaluated under the enhanced attacks. Our watermarking method still demonstrates superior robustness across all attack types and datasets, ranking either first or second. Figure 8 shows TPR@0.1%FPR versus the number of rows under three representative and strong attacks with higher strength setting. Among eight out of fifteen cases, our method reaches 1.0 TPR@0.1%FPR using only 400 rows, with the remaining seven requiring fewer than 1K rows. In contrast, baseline methods often suffer reduced true positive rates or completely lose detectability under these conditions.

To provide a more comprehensive view of robustness, we include additional empirical results under row deletion and column deletion attacks with varying deletion strengths in Figure 9. The results show that our method ranks first or second across most attack levels, demonstrating strong resilience even under high-strength attacks.

G.4 Privacy-Enhanced TAB-DRW Evaluation

Data fidelity vs. watermark detectability. Table 21 shows that privacy-enhanced TAB-DRW achieves consistently high data fidelity and detectability across three randomly sampled keys. Although minor variations exist, they remain within an acceptable range, indicating that users need not devote much effort to tuning the key. Additionally, the empirical results further strengthen our claim that the key-dependent variability in the frequency-domain representation does not substantially affect watermark distortion or detectability.

Multi-key scenarios. Under a deployment scenario with multiple watermark key holders, we evaluate potential key collision, i.e., how many different keys κ in Algorithm 2 & 3 can be used for a dataset without leading to false positives during detection. In practice, there exists an upper bound on the number of watermark keys that can be supported without introducing elevated false positives. And this capacity is influenced by the number of dataset columns. The cross-key confusion matrices in Table 22 present empirical results on the ability to detect and distinguish between different watermark keys, demonstrating the superiority of our method in avoiding potential key collisions in multi-user scenarios.

Table 22: Multi-key evaluation on five benchmarks. The randomly selected keys along the horizontal axis are used for sampling, while those along the vertical axis are used for detection: FPR/TPR(diagonal) of 1K independent trials under threshold $q_\alpha = 6$ on 1K rows.

Dataset	Detection key	Sampling keys				
		Key 48	Key 275	Key 496	Key 643	Key 928
Adult	Key 48	1.000	0.000	0.000	0.000	0.000
	Key 275	0.000	0.998	0.000	0.000	0.000
	Key 496	0.000	0.000	1.000	0.001	0.000
	Key 643	0.000	0.007	0.000	0.996	0.000
	Key 928	0.000	0.000	0.000	0.000	1.000
Magic	Key 48	1.000	0.000	0.000	0.000	0.000
	Key 275	0.000	1.000	0.000	0.000	0.000
	Key 496	0.000	0.000	1.000	0.001	0.000
	Key 643	0.000	0.000	0.000	1.000	0.000
	Key 928	0.000	0.000	0.000	0.000	1.000
Shoppers	Key 48	1.000	0.000	0.000	0.000	0.000
	Key 275	0.000	1.000	0.000	0.000	0.000
	Key 496	0.000	0.000	1.000	0.000	0.000
	Key 643	0.000	0.000	0.000	1.000	0.000
	Key 928	0.000	0.000	0.000	0.000	1.000
Default	Key 48	1.000	0.000	0.000	0.000	0.000
	Key 275	0.002	1.000	0.000	0.000	0.000
	Key 496	0.000	0.000	1.000	0.000	0.000
	Key 643	0.000	0.000	0.000	1.000	0.000
	Key 928	0.000	0.000	0.000	0.000	1.000
Drybean	Key 48	1.000	0.000	0.000	0.000	0.000
	Key 275	0.000	1.000	0.000	0.000	0.000
	Key 496	0.000	0.000	1.000	0.000	0.000
	Key 643	0.000	0.000	0.000	1.000	0.004
	Key 928	0.000	0.000	0.000	0.000	1.000

H Discussion and Future Work

Several directions remain open for future work. First, it is worth exploring whether there exists a provably optimal strategy for modifying the DFT components to maximize detectability while minimizing distortion—and if so, in what sense. Second, integrating TAB-DRW with differential privacy or membership inference protections could provide unified mechanisms for data traceability and privacy preservation. Third, adapting the watermark strength based on feature importance or downstream task performance could further improve the fidelity–detectability trade-off. We hope these directions inspire further research toward robust and responsible use of synthetic tabular data.